Physics – Uspekhi **59** (3) 225 – 253 (2016)

60th ANNIVERSARY OF THE JOINT INSTITUTE FOR NUCLEAR RESEARCH

PACS numbers: **13.15.+g**, 14.60.Lm, 14.60.Pq, 14.60.St, **26.65.+t**

Neutrino physics and JINR

V A Bednyakov, D V Naumov, O Yu Smirnov

DOI: 10.3367/UFNe.0186.201603b.0233

Contents

Abstract. The current status of neutrino physics is briefly reviewed, the basic properties of the neutrino are discussed, and the most challenging problems in this rapidly developing field are described. Written to mark the anniversary of the Joint Institute for Nuclear Research, this paper highlights JINR's contributions to the development of neutrino physics and places special emphasis on the prospects of the JINR neutrino program.

Keywords: neutrino, neutrino oscillations, neutrino mass, mass hierarchy, CP invariance violation, Majorana neutrino, reactor antineutrino, solar neutrino, atmospheric neutrino, accelerator neutrino, geo-neutrino, astrophysical neutrino, relic neutrino

1. What we know about neutrinos

Neutrino physics has taken a dramatic path from an ingenious theoretical surmise, through the difficulties of experimental discovery and various 'questions' and 'puzzles', to systematic studies of neutrino properties and the use of these particles as a unique research tool in elementary particle physics, astrophysics, cosmology, geophysics, neutrino astronomy, and applied physics. The neutrino rightfully occupies one of the leading places in modern science. These particles, which violate parity in weak interactions, indicated the correct gauge symmetry group of the Standard Model (SM), and the main hopes of discovering a 'new physics' beyond the SM are currently related exactly to neutrinos.

To date, a large amount of experimental data is accumulated concerning observation of neutrinos from different sources. In this paper, we focus on what is already known about the neutrino and what is still to be found and how. A detailed description of neutrino experiments can be found, e.g., in reviews [1–7] published in *Physics–Uspekhi* in 2014 and dedicated to the centennial of the birth of B M Pontecorvo. Results of studies of long-baseline neutrino oscillations with particle accelerators are reported in review [8], and unresolved issues of particle physics are discussed in [9].

1.1 History of the neutrino

In 1896, A Becquerel discovered radioactivity when studying the phosphorescence of potassium uranil sulfate. Two years later, Pierre and Marie Curie discovered two other radioactive nuclei, later named polonium and radium. In 1903, all three researchers were awarded the Nobel prize for the discovery of radioactivity. By that time, E Rutherford and F Soddy formulated the theory of atomic decays, which put an end to the ancient idea of indivisible atoms, and three types of radioactive decays, differing by the electric charge and the penetrating power of radiation emitted in these decays, were named α-, β-, and γ-radioactivity. Now we know that α-, β-, and γ-rays represent nuclei of helium, electrons, and photons. These particles appear due to spontaneous fission of nuclei in strong, weak, and electromagnetic decays.

According to quantum mechanics, the energy of these particles should correspond to the difference between energy levels of the initial and final nuclei. Indeed, α- and γ-radioactive decays with discrete spectra of emitted particles beautifully fit this paradigm, whereas a continuum spectrum of emerging β-particles clearly violated the expected discreteness of the energy spectrum. This phenomenon, discovered by J Chadwick in 1913, greatly puzzled physicists of the day,

V A Bednyakov, D V Naumov, O Yu Smirnov
Joint Institute for Nuclear Research,
ul. Joliot-Curie 6, 141980 Dubna, Moscow region, Russian Federation
E-mail: vadim.bednyakov@jinr.ru,
dmitryvnaumov@gmail.com,
osmirnov@jinr.ru

Received 27 July 2015, revised 27 September 2015
Uspekhi Fizicheskikh Nauk **186** (3) 233 – 263 (2016)
DOI: 10.3367/UFNr.0186.201603b.0233
Translated by K A Postnov; edited by A M Semikhatov

because at that time it seemed to violate the energy conservation law. Niels Bohr was ready to abandon the energy conservation law at the microscopic level, having the energy conserved only on average. Bohr held this view until 1936.

Another problem in the early 20th century, which at first glance was unrelated to the energy conservation violation, was the 'incorrect' statistics of the $^{14}_{7}$N and $^{6}_{3}$Li nuclei. At that time, the atomic nucleus was thought to consist of protons and electrons. Correspondingly, a $^{14}_{7}$N nucleus should contain 14 protons and 7 electrons. The odd number of fermions in the $^{14}_{7}$N nucleus should lead to the Fermi statistics for that nucleus, which contradicted experimental data clearly suggesting that the $^{14}_{7}$N nucleus follows the Bose statistics. This problem was called the 'nitrogen catastrophe'.

Pauli, in his famous letter to 'radioactive ladies and gentlemen' of 1930, assumed that there is a light neutral particle inside the nucleus with a mass of less than one hundredth the proton mass. The existence of such a particle, which Pauli called the neutron, would enable simultaneous solution of both problems: the continuous β-spectrum and the nitrogen catastrophe.

Indeed, in β-decays, Pauli's 'neutron' should be emitted together with an electron, carrying away a fraction of the β-decay energy to keep the sum of energies of the electron and neutron constant. To avoid detection, Pauli's neutron should interact very weakly. The 'incorrect' statistics of $^{14}_{7}$N was also explained quite naturally. The nitrogen nucleus consists of 14 protons, 7 electrons, and an odd number of neutrons that should be assumed to have spin 1/2.

Pauli's hypothesis was very bold, because only three elementary particles were known at that time: the proton, the electron, and the photon. We now know that to solve the continuous β-spectrum problems and the nitrogen catastrophe, one particle, Pauli's neutron, is insufficient. Two different particles are required.

The nitrogen catastrophe is explained by the absence of electrons in the nucleus: the $^{14}_{7}$N nucleus consists of 7 protons and 7 neutrons. The neutron, discovered by Chadwick in 1932, turned out to be heavier than the proton. The even total number of protons and neutrons leads to the Bose statistics for nitrogen nucleus $^{14}_{7}$N.

The continuity of the β-spectrum is then explained by a light particle ejected together with an electron and carrying away some energy. E Fermi dubbed Pauli's neutron the 'neutrino' ('small neutron' in Italian). In 1933, Pauli reported his hypothesis at the Solvay Conference in Brussels. In two months, Fermi formulated the quantum theory of β-decay, but his paper was rejected by the journal *Nature* as "abstract assumptions, too far from reality to be interesting to the readers." Fermi's theory was published in 1934 in *Zeitschrift für Physik*. The lack of interest in this paper prompted Fermi to take up experimental physics [10].

Antineutrinos were first detected in 1956 in experiment by Reines and Cowan [11], who registered $\bar{\nu}_e$ interactions from a nuclear reactor in the inverse β-decay reaction ($\bar{\nu}_e + p \to n + e^+$) in a liquid scintillator (LS) with dissolved cadmium salts. The reaction products, a positron and a neutron, carry a specific time 'tag' in the detector. The positron, after having lost its kinetic energy in the ionization process, annihilates with an electron in the medium to generate two γ quanta, each with the energy of 511 keV, which gives rise to a scintillation flash, narrow in time, detected by photoelectron multiplier tubes (PMTs). The neutron, thermalized due to collisions with nuclei of the medium, is captured by a proton or a cadmium nucleus, and several γ quanta with an energy of a few MeV are then emitted. As a result, in a characteristic time of the order of 100 μs, another oscillation flash appears, which is also detected by PMTs. For the experimental detection of antineutrinos, Reines was awarded the Nobel Prize in 1995 (Cowan had passed away before the prize was awarded). The method of detection of reactor antineutrinos applied by Reines and Cowan became the standard method of antineutrino detection.

In 1962, L Lederman, M Schwartz, and J Steinberger discovered another type of neutrino, the muon neutrino ν_μ, in an experiment on pion decay $\pi^+ \to \mu^+ + \nu_\mu$ [12]. Pions were produced in deep inelastic scattering of protons accelerated in the cyclic accelerator at Brookhaven. The particles were registered by a spark camera. The experimentalists were able to reliably distinguish muons from electrons using particle tracks. The detector was screened by a 13 m steel layer from all products of the interaction of protons with the target except from neutrinos, which easily penetrated the steel and could sometimes interact in the spark camera. Ultimately, it was found that neutrinos from pion decays generate muons and not electrons, i.e., two different types of neutrinos were discovered [12]. In 1988, Lederman, Schwartz, and Steinberger were awarded the Nobel Prize for the discovery of the muon neutrino and the suggested method of obtaining a neutrino beam, which has now become standard for producing accelerator neutrino beams.

The third neutrino type, the τ-neutrino ν_τ, was discovered in 2000 in an experiment carried out by the DONUT (Direct Observation of the NU Tau) collaboration, in which ν_τ from D_s-meson decays were registered in nuclear photoemulsion. In total, four ν_τ-events were detected with the expected number of the background events less than 0.2 [13]. In 2007, the DONUT collaboration reported [14] the detection of nine ν_τ-events already, and these statistics for the first time allowed an experimental estimation of the interaction cross section of ν_τ with a nucleon.

Weak interactions violate the spatial parity, or P-parity, which shows up, for example, in decays of polarized particles in the form of experimental correlations between the flight direction of final particles and the polarization vector of the decaying particle. The spatial parity violation was first demonstrated in 1957 in Wu's experiment with unstable cobalt isotope decay [15]

$$^{60}_{27}\mathrm{Co} \to {}^{60}_{28}\mathrm{Ni} + e^- + \bar{\nu}_e + 2\gamma\,.$$

This experiment revealed that electrons prefer to escape in the direction opposite to the cobalt nucleus spin, which means parity violation.

This revolutionary discovery, which was hard to accept by many physicists, led to the recognition that the electroweak part of the SM (which we discuss in Section 1.2) should be constructed using left chiral fields. In 1957, theoreticians Lee and Yang, who had proposed searching for the parity violation in weak decays, were awarded the Nobel Prize.

Thus, in the period from 1956 to 2000, three types of neutrinos, ν_e, ν_μ, and ν_τ, were found. The quantum number corresponding to each neutrino flavor seemed to be strictly conserved until neutrino oscillations, the phenomenon where

the flavor is not conserved,[1] were discovered. Thus, it was established that a neutrino with a certain flavor is not a particle with a certain mass, but represents a quantum superposition of massive neutrino states. Experimental confirmations of neutrino oscillations were awarded the Nobel Prize in 2015. The leader of the Super-Kamiokande (Super-Kamioka Neutrino Detection Experiment), Takaaki Kajita, was awarded this prize for the discovery of atmospheric neutrino oscillations, and the leader of the SNO (Sudbury Neutrino Observatory), Arthur Macdonald, was awarded a Nobel Prize for the confirmation of solar neutrino oscillations.

Neutrino oscillations were first predicted by B M Pontecorvo in 1957, long before their experimental confirmation. We note that Pontecorvo showed astonishing intuition and farsightedness by suggesting a method of neutrino detection, successfully realized in the chlorine–argon experiment by Davis [16]. Pontecorvo suggested that the neutrinos discovered by Raines and Cowan and neutrinos from pion decays should be two different particles, which was beautifully confirmed in the experiment by Lederman, Schwartz, and Steinberger. Pontecorvo also put forward the idea of the universality of weak interactions. He and M A Markov, when working at the Joint Institute for Nuclear Research (JINR), laid the foundation for the neutrino school in Dubna and in the Soviet Union. The modern neutrino research program at JINR is discussed in Section 3.

1.2 Standard Model: basics of the theory and mixing of fermions

Today, all the diversity of particle physics is perfectly described by the Standard Model — a quantum field theory with the gauge symmetry group $\mathrm{SU(3)_c \times SU(2)_L \times U(1)_Y}$.

The SM has a large number of free parameters, including particle masses and coupling constants; however, it uniquely predicts the form of interactions. These predictions are in impressive agreement with experiment. In the initial formulation of the SM developed in the mid-1970s, neutrinos were assumed to be massless, which did not contradict the experimental data of that time. As a result, the lepton number conservation was predicted. This theory is sometimes referred to as the minimal SM. The introduction of nonzero neutrino masses, in analogy with quarks, minimally extends the SM. In the literature, this version of the SM is sometimes called the νSM. In this paper, we prefer to refer to both these variants of the SM equally as the SM, because the key prediction, the form of interactions, remains unchanged in both models. In this respect, our terminology differs from the one used in [9], where the presence of mixing and different neutrino masses are treated as deviations from the SM.

By contrast, any nontrivial extension of the SM related to the change of the form of interactions or the introduction of new particles that are absent in the SM is classified in this paper as physics Beyond the Standard Model (BSM). Presently, the strongest indication of the incompleteness of the SM comes from cosmological data, which require, for example, the presence of dark matter and dark energy, as well as violation of the baryon number conservation. Many particle physicists, cosmologists, and astrophysicists are searching for experimental evidence of physics BSM.

The electroweak part of the SM is based on the gauge symmetry of interactions under transformations of the group $\mathrm{SU(2)_L \times U(1)_Y}$. The SM Lagrangian includes a kinetic term describing free propagation of fermions and their interaction with gauge bosons, the Higgs potential with a minimum at a nonzero value of the Higgs field, and the Yukawa potential of fermions coupled to the Higgs field. The gauge invariance of the SM Lagrangian requires zero masses of fermions and gauge bosons, which, clearly, is far from the reality. The vector $\mathrm{W^{\pm}}$ and Z bosons and fermions acquire mass due to spontaneous gauge symmetry breaking, when the Higgs potential attains a minimum at a nonzero vacuum expectation value of the scalar Higgs field. The discovery of the Higgs boson in 2012 in the Large Hadron Collider (LHC) experiments [17] was a triumph of the theoretical ideas.

As in the general case, the Yukawa potential mixes fermions of different flavors; the mass eigenstates are mixed in interactions with $\mathrm{W^{\pm}}$ bosons. This mixing is described by the Cabbibo–Kobayashi–Maskawa (CKM) mixing matrix for quarks and the Pontecorvo–Maki–Nakagawa–Sakata (PMNS) mixing matrix for leptons (also known as the neutrino mixing matrix). Both matrices should be unitary. The lepton mixing matrix is usually parameterized by three mixing angles θ_{ij} and phase δ responsible for CP violation:

$$V = \begin{pmatrix} 1 & 0 & 0 \\ 0 & c_{23} & s_{23} \\ 0 & -s_{23} & c_{23} \end{pmatrix} \begin{pmatrix} c_{13} & 0 & s_{13}\exp(-\mathrm{i}\delta) \\ 0 & 1 & 0 \\ -s_{13}\exp(\mathrm{i}\delta) & 0 & c_{13} \end{pmatrix} \times \begin{pmatrix} c_{12} & s_{12} & 0 \\ -s_{12} & c_{12} & 0 \\ 0 & 0 & 1 \end{pmatrix}, \quad (1)$$

where $c_{ij} \equiv \cos\theta_{ij}$ and $s_{ij} \equiv \sin\theta_{ij}$. Mixing and different masses of neutrinos result in the lepton number nonconservation. If the lepton number were conserved, the following reaction could be possible:

$$\pi^+ \to \mu^+ + \nu \hookrightarrow \nu + n \to p + \mu^-, \quad (2)$$

while the reaction

$$\pi^+ \to \mu^+ + \nu \hookrightarrow \nu + n \to p + e^- \quad (3)$$

would be impossible. Mixing in the lepton part of the SM makes it possible that a neutrino produced in the $\pi^+ \to \mu^+ + \nu_\mu$ decay as a muon neutrino, after passing some macroscopic distance, with some probability appears as a neutrino with a different flavor, for example, as an electron neutrino, which can participate in reaction (3).

1.3 Neutrino oscillations in the vacuum and in matter

1.3.1 Vacuum oscillations. Transformation of the flavor of a neutrino depends periodically on the ratio L/E_ν of the path of the neutrino L to its energy E_ν. This phenomenon is known as neutrino oscillations.

The characteristic oscillation length is $L_{ij}^{\mathrm{osc}} = 4\pi E_\nu/|\Delta m_{ij}^2|$, where $\Delta m_{ij}^2 = m_i^2 - m_j^2$ is the difference between the neutrino mass squares. The basic theory of neutrino oscillations was formulated by Pontecorvo and S M Bilen'ky at JINR.

[1] Here and below, we consider not quark flavors but lepton flavors. Lepton flavor is a convenient general term for three lepton charges: electron, muon, and tau. It should be noted that presently there is no experimental evidence that the total lepton flavor is not conserved, although there are SM extensions predicting its nonconservation.

In a simplified way, neutrino oscillations can be described as follows. Let a reaction with the participation of a charged W-boson produce an antilepton ℓ_α^+ $(\alpha = \mathrm{e}, \mu, \tau)$ and a neutrino with a certain flavor, which is a superposition of mass states ν_i: $\nu_\alpha = \sum_i V_{\alpha i}\nu_i$, where $V_{\alpha i}$ are elements of mixing matrix (1). The mass state ν_i evolves in time in accordance with the Schrödinger equation $\nu_i(t) = \exp(-\mathrm{i}E_i t)\nu_i$, and this results in $\nu_\alpha(t) \neq \nu_\alpha$ if the neutrinos have different masses. Thus, the original state with a certain flavor changes in time, and there is a nonzero probability of discovering a quantum admixture of a neutrino with another flavor β and, as a consequence, the production of the lepton ℓ_β^- with another flavor.

The probability that the original flavor α of a neutrino with the energy E_ν is preserved after passing a length L in the vacuum, is in the plane-wave approximation given by

$$P_{\alpha\alpha} = \sum_{i,j} |V_{\alpha i}|^2 |V_{\alpha j}|^2 \exp\left(-\mathrm{i}\frac{\Delta m_{ij}^2 L}{2E_\nu}\right), \tag{4}$$

whereas the probability of the flavor change $\alpha \to \beta$ in the same approximation is

$$P_{\beta\alpha} = \sum_{i,j} V_{\alpha i}^* V_{\beta i} V_{\alpha j} V_{\beta j}^* \exp\left(-\mathrm{i}\frac{\Delta m_{ij}^2 L}{2E_\nu}\right). \tag{5}$$

Here, it is appropriate to raise the following question. In analogy with the flavor oscillations considered above, in which two charged leptons ℓ_α^+ and ℓ_β^- label the process, we can theoretically require that two massive neutrino states, ν_i and ν_j, be respectively distinguished in the source and in the detector. Should we then expect that instead of a charged lepton with a certain flavor, we discover a quantum mixture $\ell_i = \sum_\alpha V_{\alpha i}\ell_\alpha$ and, as a consequence, an oscillation of charged leptons? This question is all the more relevant because the mixing matrix V is assigned to the neutrino by convenience, while in reality it is a common lepton mixing matrix. Charged leptons and neutrinos enter the corresponding SM Lagrangian in a symmetric way.

The correct theoretical description of neutrino oscillations requires the use of wave packets for neutrinos[2] to define the notion of the neutrino path length and to resolve some inconsistencies in the plane wave formalism.

The wave packet approach predicts a number of observational effects, such as the condition for coherent formation of a superposition of mass states and the loss of coherence at distances exceeding the coherence length of neutrino oscillations. This treatment also explains why charged leptons do not oscillate [31]: in most of the practical cases, the difference between charged lepton mass squares turns out to be too large for the charged leptons to be produced in a coherent quantum mixture.

Neutrino oscillations proved to be a very sensitive tool to measure the difference between the neutrino mass squares Δm_{ij}^2 and the mixing angles θ_{ij}. Neutrino oscillations have been reliably detected in many experiments with different sources: accelerator, reactor, solar, and atmospheric. Figures 1–3 present survival probabilities of neutrinos as a function of the ratio L/E_ν as measured by the Super-Kamiokande [32], KamLAND (Kamioka Liquid-scintillator Antineutrino Detector) [33], and Daya Bay [34] experiments, which are mainly sensitive to vacuum neutrino oscillations, with negligible matter effects.

[2] In the quantum mechanical treatment of neutrino oscillations, where all particles except neutrinos are ignored, the wave packet for neutrinos is postulated [18–25]. Another approach uses quantum field theory to calculate the entire process from neutrino production to its detection. There, neutrinos themselves are treated as virtual particles. The neutrino wave function is not postulated but is calculated as a function of all particles participating in the reaction [26–30].

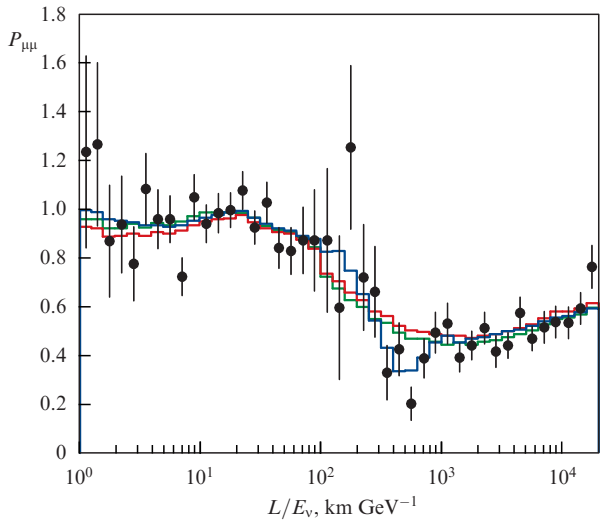

Figure 1. (Color online.) Survival probability of muon neutrinos $P_{\mu\mu}$ as a function of L/E_ν (neutrino path length/neutrino energy). Dots with error bars represent the Super-Kamiokande measurements. The blue curve shows the neutrino oscillation theory prediction. (From Ref. [32].)

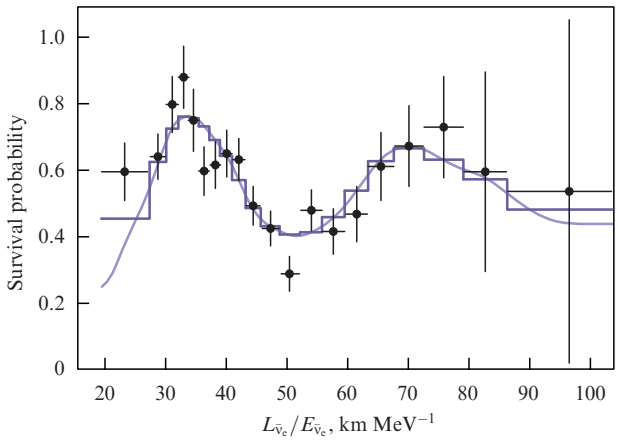

Figure 2. Survival probability of electron antineutrinos as a function of $L_{\bar{\nu}_e}/E_{\bar{\nu}_e}$ (antineutrino path length/antineutrino energy). Dots with error bars show the KamLAND collaboration measurements after subtraction of the geoneutrino background. The histogram and solid curve show the neutrino oscillation theory prediction for oscillation parameters derived from the KamLAND data. (From Ref. [33].)

1.3.2 Neutrino oscillations in matter. When neutrinos pass through ordinary matter, an asymmetry between the propagation of electron neutrinos and neutrinos of other flavors arises because ν_e scatters on electrons of the medium by exchanges of W^+ and Z bosons, while ν_μ and ν_τ are scattered on the medium electrons only due to Z-boson exchanges.

The potential energy of elastic $\nu_e e$ scattering, which is $\sqrt{2}G_F n_e \sim 10^{-10} - 10^{-11}$ eV in the solar center (here, G_F is the

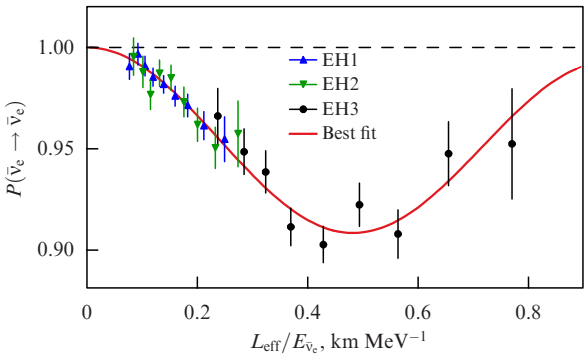

Figure 3. Survival probability of electron antineutrinos as a function of $L_{\text{eff}}/E_{\bar{\nu}_e}$ (antineutrino path length/antineutrino energy). Triangles pointing up and dots with error bars show the Daya Bay collaboration measurements in different experimental rooms, EH1, EH2, and EH3 respectively. The solid curve indicates the neutrino oscillation theory predictions. (From Ref. [34].)

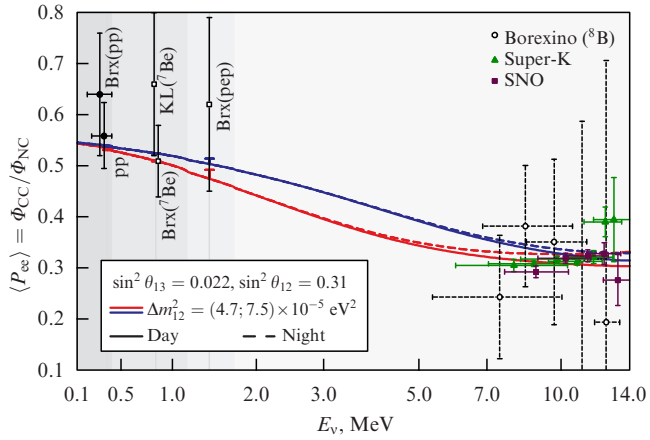

Figure 4. Survival probability of solar electron neutrinos $\nu_e^{\odot}$ as a function of the neutrino energy E_ν. Φ_{CC} is the electron neutrino flux and Φ_{NC} is the total neutrino flux. Symbols with error bars are experimental data. The line with the uncertainty band is the theoretical prediction in the neutrino oscillation model in matter. Brx(...) is the survival probability of the corresponding neutrino flux $\nu_e^{\odot}$ obtained from the Borexino experiment. KL (^{7}Be) is the survival probability of the $\nu_e^{\odot}$ flux from the ^{7}Be reaction according to the KamLAND experiment. (Super-K — Super-Kamiokande.) (From Ref. [37].)

Fermi constant and n_e is the electron number density), is small compared to the characteristic energies of the solar neutrinos of the order of a few MeV. However, it would be incorrect to ignore the electron scattering effect on neutrino oscillations. The interaction energy turns out to be of the same order as the energy difference $\Delta E_{ij} = \Delta m^2_{ij}/2E_\nu$ determining neutrino oscillations in the vacuum for Δm^2, of the order of $(10^{-4} - 10^{-5})$ eV, and E_ν of about a few MeV. Hence, matter can significantly affect neutrino oscillations. Qualitatively, the matter effect is that the mixing angles and neutrino mass values in a medium differ from vacuum values and depend on the electron number density and the energy of neutrinos. Correspondingly, eigenstates $\tilde{\nu}_i$ of the Hamiltonian in matter differ from the eigenstates ν_i in the vacuum. (The parameters of neutrinos in matter, such as mixing angles, mass, and energy, are indicated with a tilde in what follows.)

In this connection, we qualitatively discuss theoretical expectations for the survival probability of solar electron neutrinos. Neutrinos with energies below 1 MeV are virtually insensitive to the matter effect on oscillations. Their propagation is determined by vacuum oscillations. When detecting the neutrino flux on Earth, averaging along the neutrino path (inside the Sun, on the way from the Sun to the detector, etc.) cancels the interference term in the probability formula, which results in the electron neutrino survival probability $\langle P_{ee}\rangle = 1 - (1/2)\sin^2(2\theta_{12})$ if the mixing angle θ_{13} is ignored for simplicity. At neutrino energies of the order of 1.5–2.0 MeV for neutrinos generated in the solar center, the so-called Mikheev–Smirnov–Wolfenstein (MSW) resonance [35, 36] appears, which leads to oscillations with a maximum amplitude on the characteristic scale of several hundred kilometers and ultimately results in equal numbers of electron and muon neutrinos, or $\langle P_{ee}\rangle \approx 1/2$.

For neutrinos with the energy above 6–8 MeV, the matter effects are so strong that the state of electron neutrinos at the solar center virtually coincides with the neutrino energy eigenstate in matter $\tilde{\nu}_2$ and remains in this state until the exit from the Sun, with gradual transformation to the vacuum state ν_2. The impossibility of a transformation into another mass state when propagating in a medium with variable density is determined by the adiabaticity condition $\mathrm{d}\tilde{\theta}(t)/\mathrm{d}t \ll \Delta\tilde{E}_{12}$, which holds for all energies of solar neutrinos with good accuracy. Hitting the neutrino detector on Earth, ν_2 interacts with an electron with a probability proportional to $\sin^2\theta_{12}$. Therefore, the survival probability in this case is $\langle P_{ee}\rangle = \sin^2\theta_{12}$.

For intermediate neutrino energies of 2–6 MeV, two effects, the MSW resonance and adiabatic conversion, are combined. At energies about 2 MeV, the NSW resonance still plays a significant role, and $\langle P_{ee}\rangle \simeq 1/2$ at these energies. With the energy increasing from 2 MeV to $\simeq 6$ MeV, the role of adiabatic conversion gradually increases, which smoothly leads to $\langle P_{ee}\rangle = \sin^2\theta_{12}$.

All features discussed above are seen in the theoretical curve (Fig. 4), which matches the experimental results well.

The survival probability of solar ν_e is sensitive to the sign of Δm^2_{21}. A comparison of theoretical results with experiments suggests that $\Delta m^2_{21} > 0$, i.e., ν_2 is heavier than ν_1. Today, it is unknown which state, ν_1 or ν_3, is heavier. Table 1 lists the most reliable current values of the mixing angles and the differences between neutrino mass squares as derived from global data analysis [38][3] for two possible mass hierarchies: the normal one, $m_3 > m_1$, and the inverted one, $m_1 > m_3$.

1.4 Number of neutrino flavors

In the SM, the widths of $W^{\pm}$- and Z-boson decays are sensitive to the number of neutrino flavors. Three generations of leptons provide about 30% and 20% of the total widths of $W^{\pm}$ and Z bosons, respectively. Figure 5 presents the interaction cross section of $e^+e^- \to$ hadrons as a function of the total energy of the colliding particles measured in the LEP (Large Electron–Positron collider) experiments [40]. The experimental results are compared to SM calculations with 2, 3, and 4 neutrino flavors. The best agreement with experiments is obtained for $N_\nu = 2.984 \pm 0.008$, in agreement with three generations. The existence of weakly interacting particles with quantum numbers of neutrinos and masses greater than $m_Z/2$ is not excluded from the analysis of Z-boson decays.

[3] There are other global neutrino oscillation data analyses. The interested reader can find the results in the Review of Particle Properties [39].

Table 1. Oscillation parameters from the global fit to oscillation experiment data in the three-flavor neutrino model.* (From Ref. [38].)

Parameter	Value for NH	Value for IH
Δm^2_{21}	$(7.54^{+0.26}_{-0.22}) \times 10^{-5}$ eV^2	$(7.54^{+0.26}_{-0.22}) \times 10^{-5}$ eV^2
$\Delta m^2 = m^2_3 - (m^2_1 + m^2_2)/2$	$(2.43 \pm 0.06) \times 10^{-3}$ eV^2	$(2.38 \pm 0.06) \times 10^{-3}$ eV^2
$\sin^2\theta_{12}$	0.308 ± 0.017	0.308 ± 0.017
$\sin^2\theta_{13}$	$0.0234^{+0.0020}_{-0.0019}$	$0.0240^{+0.0019}_{-0.0022}$
$\sin^2\theta_{23}$	$0.437^{+0.033}_{-0.023}$	$0.455^{+0.039}_{-0.031}$
δ/π	$1.39^{+0.38}_{-0.27}$	$1.31^{+0.29}_{-0.33}$

* Values for the normal and inverted mass hierarchy (NH and IH, respectively) are presented. The value Δm^2 is positive for NH and negative for IH. The fitting results suggest that modern experiments cannot distinguish between the mass hierarchies, the χ^2 difference for the normal and inverted hierarchies being 0.3.

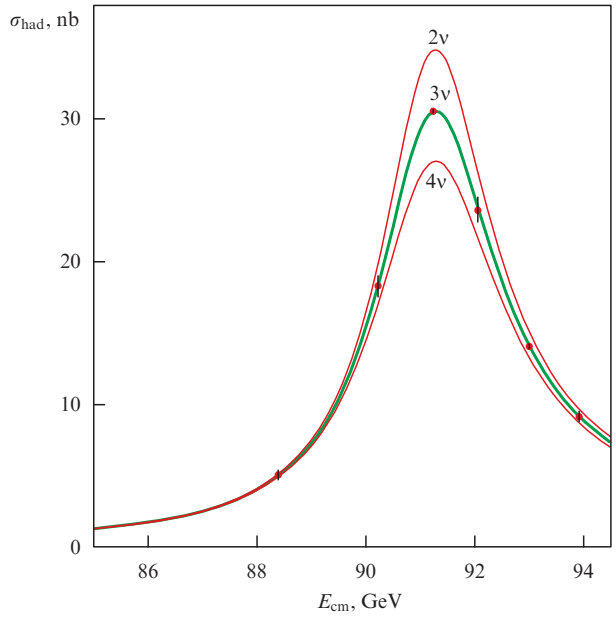

Figure 5. Cross section of $e^+e^- \to$ hadrons as a function of the total energy E_{cm} in the center-of-mass system of a colliding e^+e^- pair measured in the ALEPH (Apparatus for LEP Physics), DELPHI (Detector with Lepton, Proton, and Hadron Identification), L3, and OPAL (Omni-Purpose Apparatus at LEP) experiments (dots with error bars are blown up 10-fold for visibility), and theoretical calculations in the SM framework (solid curves) with 2, 3, and 4 neutrino generations. (From Ref. [40].)

In 2015, the Planck collaboration published an estimate of the effective number of relativistic degrees of freedom[4] (with the exception of photons) in the primordial plasma in the early Universe, $N_\nu = 3.15 \pm 0.23$ [41], as inferred from the temperature and polarization measurements of the cosmic microwave background and other astrophysical data. Usually, this number is related to the number of neutrino species.

We note that it is possible to introduce additional neutrino fields in the SM, such that they do not contribute to the observed widths of the $W^\pm$- and Z-boson decays, if the masses of these fields are small compared to the vector boson masses; however, they then show up as relativistic degrees of freedom in plasma in the early Universe. These fields would also manifest themselves in other processes, including neutrino oscillations, and would contribute to the effective neutrino masses in weak particle decays. This possibility is related to so-called sterile neutrinos, which are discussed in Section 2.4.

[4] A thermodynamic consideration of the primordial plasma in the Universe suggests that the effective number of relativistic degrees of freedom of neutrinos need not necessarily be an integer.

1.5 Neutrino mass

The observed neutrino oscillations suggest that at least two of the three neutrino mass states have a nonzero mass, which allows imposing lower bound on the neutrino mass. Based on the data in Table 1, it is possible to assert that the heaviest neutrino must have a mass not less than $|\Delta m^2_{13}|^{1/2} \simeq 0.05$ eV, and the next heavy neutrino mass should be at least $|\Delta m^2_{21}|^{1/2} \simeq 0.009$ eV. However, neutrino oscillations do not put upper bounds on the possible neutrino masses. Some observables are sensitive to the neutrino mass scale. In β-decays of particles, the maximum possible energy of the decay products depends on the neutrino masses:

$$m^2_{\nu_\alpha} = \sum_i |V_{\alpha i}|^2 m^2_i\,, \qquad \alpha = e, \mu, \tau\,. \tag{6}$$

An experiment in Troitsk, Russia, put the best upper bounds on m_{ν_e} from an analysis of tritium decays $^3H \to {}^3He + e^- + \bar{\nu}_e$ [42]:

$$m_{\nu_e} < 2.05 \text{ eV } (95\% \text{ CL}) \tag{7}$$

(CL is the confidence level). Pion decays $\pi^+ \to \mu^+ + \nu_\mu$ put less stringent constraints on the muon neutrino mass [43]:

$$m_{\nu_\mu} < 170 \text{ keV } (90\% \text{ CL})\,. \tag{8}$$

A kinematic analysis of τ-lepton decay with three or five charged pions in the final state yields much looser bounds on the τ-neutrino mass [44]:

$$m_{\nu_\tau} < 18.2 \text{ MeV } (95\% \text{ CL})\,. \tag{9}$$

The most stringent constraints on the neutrino mass are obtained from cosmology. Big Bang models predict a constant neutrino-to-photon density ratio in the Universe. If neutrinos had a mass, for example, of 50 eV, the total energy density in the Universe would exceed the critical value, which would lead to the collapse of the Universe. Therefore, measurements of the energy density in the Universe in combination with an analysis of other cosmological and astrophysical data offer a sensitive tool to constrain the total mass of all (light) neutrino species. For example, a joint analysis of the photometric catalog of more than 700,000 bright red galaxies (MegaZ DR7), the results of five-year WMAP (Wilkinson Microwave Anisotropy Probe) observa-

tions, baryonic acoustic oscillations, supernovae, and the Hubble Space Telescope data yields [45]

$$\sum_i m_i < 0.28 \text{ eV } (95\% \text{ CL}) .$$

In 2015, the Planck collaboration in combination with other cosmological data, obtained a more stringent upper bound [41]:

$$\sum_i m_i < 0.23 \text{ eV } (95\% \text{ CL}) .$$

Another interesting, albeit model-dependent, bound [46]

$$\sum_i m_i = 0.320 \pm 0.081 \text{ eV}$$

is obtained from an attempt to explain the inconsistency between cosmological parameters derived using two data sets:

— from the cosmic microwave background anisotropy (Planck, WMAP) and baryonic acoustic oscillations;

— from counting galaxy clusters using the Sunyaev–Zeldovich effect and from gravitational lensing data.

If the neutrino is a Majorana particle, the effective mass can be calculated from the lifetime of isotopes for which neutrinoless double beta decay is possible.

As of 2015, the most stringent bound is the one obtained by the KamLAND-Zen collaboration [47], in combination with the EXO-200 (Enriched Xenon Observatory 200) measurements [48] of the lifetime of the ^{136}Xe isotope: $T^{0\nu}_{1/2} > 3.4 \times 10^{25}$ years (90% CL), which corresponds to the upper bound on the effective neutrino mass $\langle m_{\beta\beta} \rangle < 0.120 - 0.250$ eV. The interval of upper bounds is due to uncertainties in theoretical calculations of the nuclear matrix elements.

With both lower bounds on the neutrino mass (from neutrino oscillations) and upper bounds (from direct bounds and cosmological data), we conclude that the masses of the heaviest and next-to-heaviest neutrinos lie within quite narrow ranges.

We also note a strong difference in the mixing matrices of neutrinos and quarks, which may suggest different mass generation mechanisms for neutrinos and quarks. This, in turn, may point to physics beyond the SM [49, 50].

1.6 Electromagnetic properties of neutrinos

The study of the electromagnetic properties of neutrinos enables directly probing many fundamental aspects of particle physics. In the SM, a neutrino at the tree level has zero electric charge and zero electric dipole and magnetic moments. Nevertheless, due to loop corrections, nonzero electromagnetic factors appear, which are, however, very small in the SM due to low neutrino masses. This is why observations of nonzero values of these properties would indicate a new physics beyond the SM. Moreover, the electromagnetic properties of neutrinos can be used to distinguish Dirac and Majorana neutrinos, because Dirac neutrinos can have nonzero values of both diagonal and off-diagonal magnetic and electric moments, while for Majorana neutrinos, only off-diagonal moments can be nonzero. A detailed consideration of the electromagnetic properties of neutrinos can be found in review [51]; below, we consider only the magnetic moment of the neutrino.

Because a neutrino of a certain flavor is a mixture of mass states, the interaction of a mass state of a neutrino with an electromagnetic field is characterized by a 3×3-matrix of dipole magnetic moments μ_{ij}. For Majorana neutrinos, the matrix μ_{ij} is antisymmetric, and only transitional off-diagonal moments can be nonzero.

The magnetic moment of the Dirac neutrino in the SM, which is proportional to the neutrino mass, is extremely small, and cannot therefore be measured in laboratory experiments:

$$\mu_\nu = \frac{3eG_F}{8\pi^2\sqrt{2}} m_\nu \simeq 3.2 \times 10^{-19} \left(\frac{m_\nu}{1 \text{ eV}}\right) \mu_B ,$$

where μ_B is the Bohr magneton and e is the electron charge.

In various extensions of the SM, the magnetic moment of the neutrino is expected to fall within the range $\mu_\nu = (10^{-11} - 10^{-12})\mu_B$ for the Majorana neutrino and $\mu_\nu < 10^{-14}\mu_B$ for the Dirac neutrino. Experimental observation of the neutrino magnetic moment with $\mu_\nu > 10^{-14}\mu_B$ would signal a new physics beyond the SM and would also evidence the Majorana neutrino. Historically, neutrino magnetic moments $\mu_\nu \simeq (10^{-11} - 10^{-10})\mu_B$ were invoked as a possible explanation of the solar neutrino deficit due to spin–flavor precession in the magnetic field of the Sun.

A nonzero magnetic moment of the neutrino would also be important for astrophysics, because it would provide an additional cooling channel for astrophysical objects. The best upper bound on the magnetic moment of the neutrino, $\mu_\nu < 3 \times 10^{-12}\mu_B$ (90% CL), was obtained from astrophysical considerations by Raffelt [52] and recently improved in [53] to $\mu_\nu < 2.2 \times 10^{-12}\mu_B$ (90% CL). Because astrophysical constraints are significantly model-dependent, this motivates experimentalists to directly search for the neutrino magnetic moment.

The most sensitive reaction from the standpoint of searches for the contribution due to a nonzero magnetic moment of the neutrino is the neutrino (antineutrino) elastic scattering on electrons. The electroweak cross section depends on the kinetic energy T_e of the scattered electron, while the electromagnetic cross section, which is proportional to the square of the magnetic moment, depends on $1/T_e$. In Fig. 6, both cross sections are plotted as a function of the kinetic energy of scattered electron T_e. It is seen that for magnetic moments of the order of $(1-6) \times 10^{-11}\mu_B$, the

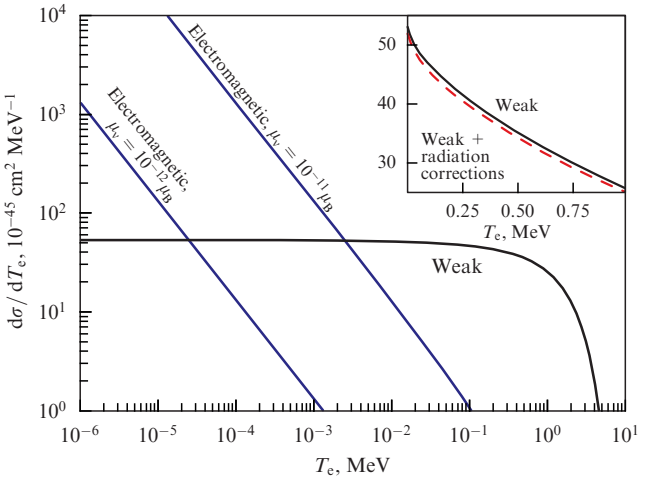

Figure 6. Electroweak, $d\sigma_W/dT$, and electromagnetic, $d\sigma_{EM}/dT$, $\nu_e e$ cross sections (for different neutrino magnetic moments) averaged over the antineutrino spectrum of fissioning ^{235}U as a function of the kinetic energy of a scattered electron. (From [54].)

electromagnetic cross section exceeds the electroweak one for energies up to $T_e \approx 3-100$ keV.

The contribution of Russian scientists to studies of the neutrino magnetic moment in nuclear reactors should be noted: for a long time, the best upper bound on the neutrino magnetic moment was

$$\mu_{\bar{\nu}_e} \leqslant 1.9 \times 10^{-10}\mu_B \ (95\% \ \text{CL}) ,$$

obtained in 1993 at Rovno Nuclear Power Plant (NPP) with a 75 kg silicon detector manufactured at the Konstantinov St. Petersburg Nuclear Physics Institute [55]. This result was insignificantly improved only ten years later in the TEXONO (Taiwan Experiment On NeutrinO) experiment [56]:

$$\mu_{\bar{\nu}_e} \leqslant 1.3 \times 10^{-10}\mu_B \ (90\% \ \text{CL}) ,$$

and in the MUNU experiment [57]:

$$\mu_{\bar{\nu}_e} \leqslant 9 \times 10^{-11}\mu_B \ (90\% \ \text{CL}) .$$

The sensitivity of measurements has been increased with time, and more stringent bounds have been obtained: from $\mu_{\bar{\nu}_e} \leqslant 10^{-9}\mu_B$ in the Raines and Cowan experiment [11] in 1957 to the most stringent bound today:

$$\mu_{\bar{\nu}_e} \leqslant 2.9 \times 10^{-11}\mu_B \ (90\% \ \text{CL}) , \qquad (10)$$

obtained in the experiment GEMMA (Germanium Experiment for Measurement of the Magnetic Moment of Antineutrino), which is run by JINR jointly with the Institute of Theoretical and Experimental Physics (ITEP) at the Kalinin NPP [58]. In the last case, the bound was derived by comparing spectra obtained with the reactor turned on and off. A 1.5 kg germanium spectrometer mounted at a distance of 13.9 m from the 3 GW reactor, where the neutrino flux is 2.7×10^{13} cm^{-2} s^{-1}, was used as the detector.

The best bound on the effective magnetic moment of solar neutrinos was obtained in the Borexino experiment [59]: $\mu_\nu^\odot \leqslant 5.4 \times 10^{-11}\mu_B$. Because the neutrino flux registered by Borexino is a mixture of different neutrino flavors, $\mu_\nu^\odot$ can be used to infer bounds on the magnetic moment of neutrinos with a specific flavor using oscillation parameters. The bounds are [60]

$$\mu_{\nu_e} < 7.3 \times 10^{-11}\mu_B \ (90\% \ \text{CL}) ,$$
$$\mu_{\nu_\mu}, \mu_{\nu_\tau} < 11.4 \times 10^{-11}\mu_B \ (90\% \ \text{CL}) .$$

These results should be compared with direct measurements in the GEMMA experiment [see (10)], in the accelerator experiment LSND (Liquid Scintillator Neutrino Detector), in which the magnetic moment of the muon neutrino was constrained [61] to be

$$\mu_{\nu_\mu} < 68 \times 10^{-11}\mu_B \ (90\% \ \text{CL}) ,$$

and in the accelerator experiment DONUT for the τ-neutrino [62]:

$$\mu_{\nu_\tau} < 39{,}000 \times 10^{-11}\mu_B \ (90\% \ \text{CL}) .$$

2. What we want to know about neutrinos

Despite more than half a century of studies of neutrino properties, there are a number of unsolved issues. Presently, we do not know the mass of the lightest neutrino or the neutrino mass hierarchy. The phase δ responsible for CP-violation remains unmeasured, and the sign of $\cos(2\theta_{23})$ (or the quadrant in which the angle θ_{23} lies), which is important for determining the neutrino mass hierarchy, is still unknown. So far, there has been no answer to the question of whether the neutrino is a Dirac or a Majorana particle. It is unknown whether sterile neutrinos exist. Do neutrinos have 'nonstandard' properties? What are the sources of astrophysical neutrinos detected by the IceCube experiment? Undoubtedly, the problem of the detection of relic neutrinos is a 'Nobel prize topic'. These and some other issues are very topical.

In addition to studies of the physical properties of neutrinos in dedicated experiments, the use of neutrinos in related sciences has recently become popular, in particular, in studying the chemical composition of Earth, giving rise to a new branch of science, neutrino geophysics. It is expected that the new generation of neutrino telescopes, besides providing the main measurements (detection of sources, studies of the mass hierarchy, etc.), can carry out the 'neutrino tomography' of Earth using atmospheric neutrinos, which will be an entirely new step forward in our understanding of Earth's structure.

Solar neutrino experiments in the last decade have also shifted toward studies of processes inside the Sun and solar chemical composition using neutrinos.

We can therefore assert that neutrinos have become a sensitive research tool with a huge, apparently not yet completely used, potential.

2.1 Direct measurements of neutrino mass

Noticeable experimental activity in neutrino physics in the past and at present is related to attempts to directly measure neutrino masses. The method of these measurements is based on a kinematic analysis of reactions with neutrinos. For example, in the neutron decay reaction $n \to pe^-\bar{\nu}_e$, a maximum possible energy of the final electron decreases with the mass of the antineutrino. Thus, by precisely measuring the high-energy part of the β-spectrum, it is possible to either determine the neutrino (antineutrino) mass or constrain its value.

This method was proposed by Perrin [61] and Fermi [64] almost immediately after the theory of β-decay was formulated by Fermi. In 1939, Alvarez and Cornog [65] found that tritium is a radioactive isotope with a low decay energy $Q = 18.6$ keV, which provides a relatively strong effect of the neutrino mass on the form of the β-spectrum. The use of tritium in experiments is additionally attractive because of the simplicity of calculations of atomic effects. The first tritium experiments to measure the mass of the neutrino using the kinematic method were carried out in 1949 by Hanna and Pontecorvo [66], as well as by Curran, Angus, and Cockroft [67]. These experiments established early on that the neutrino mass is very small, no more than one thousandth that of an electron.

The energy spectrum of electrons in the decay $(A, Z) \to (A, Z+1) + e^- + \bar{\nu}_e$ is determined by the noncoherent sum of partial decay widths into massive antineutrinos:

$$\frac{d\Gamma}{dT} = \sum_k |V_{ek}|^2 \frac{d\Gamma_k}{dT} , \qquad (11)$$

$$\frac{d\Gamma_k}{dT} = \frac{(G_F \cos\theta_C)^2}{2\pi^3} pp_k(T + m_e)(Q - T)|\mathcal{M}|^2 \times F(T)\theta(Q - T - m_k) , \qquad (12)$$

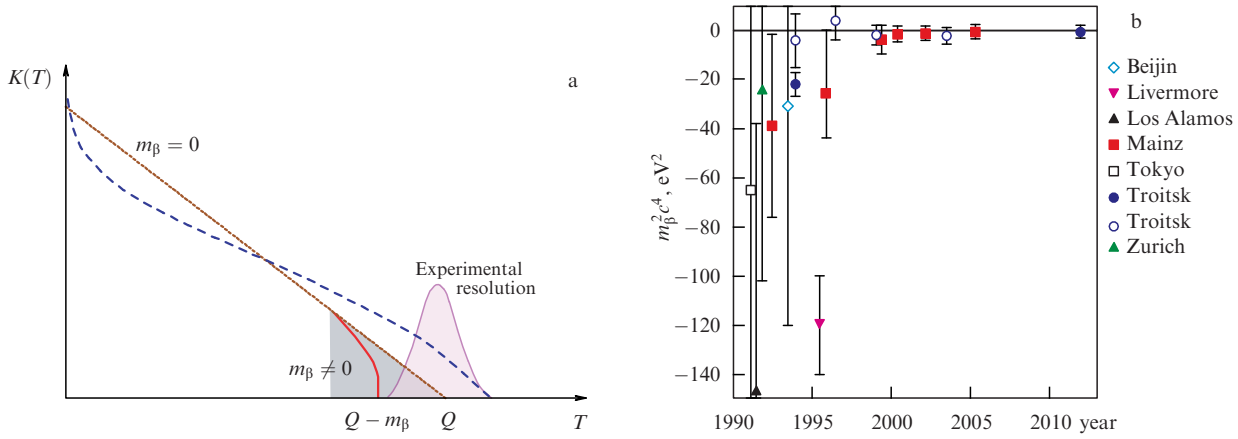

Figure 7. (a) The function $K(T)$ for $m_\beta = 0$ and $m_\beta \neq 0$. The spectrum distortion is seen at the spectral end. The characteristic experimental resolution is also shown. The real spectral shape is distorted even more strongly due to nuclear effects and the interaction of emitted electrons with particles of matter in the device. (b) The measured effective neutrino mass value m_β^2 according to experimental results published in 1990–2012 (from Ref. [69]).

where θ_C is the Cabbibo angle, m_e is the electron mass, p is the modulus of the momentum, T is the kinetic energy of the electron, $p_k = (E_k^2 - m_k^2)^{1/2} = [(Q-T)^2 - m_k^2]^{1/2}$ is the neutrino momentum, Q is the energy released in the decay (the end point of the β-spectrum in the case of a nonzero neutrino mass), $\mathcal{M}$ is the nuclear matrix element, and $F(T)$ is the Fermi function describing the Coulomb interactions of the final particles; the θ-function takes into account that the neutrino state ν_k appears only when the total energy exceeds the neutrino mass: $E_k = Q - T \geqslant m_k$.

As follows from (11), the largest deviation of the β-spectrum due to the neutrino mass can be detected in the region

$$Q - T \sim m_k \,. \tag{13}$$

However, for $\max m_k \simeq 1$ eV, only a tiny fraction (around 10^{-13}) of all decays contributes to the region in (13). Therefore, a small part of the β-spectrum is used in the analysis of the results. For example, in the tritium experiment in Mainz [68], the region with a width of 70 eV in the spectral tail was used. Taking the unitarity of the mixing matrix into account and assuming that $\max m_k^2 \ll 4(Q-T)^2$, it is possible to obtain

$$\sum_k |V_{ek}|^2 p_k \approx \sum_k |V_{ek}|^2 (Q-T)\left[1 - \frac{m_k^2}{2(Q-T)^2}\right] \approx \sqrt{(Q-T)^2 - m_\beta^2}\,,$$

where the effective neutrino mass m_β is defined as $m_\beta^2 = \sum_k |V_{ek}|^2 m_k^2$. As a result, it is possible to express the neutron decay width through the effective neutrino mass m_β, a bound for which is derived from the experiment:

$$\frac{\mathrm{d}\Gamma}{\mathrm{d}T} \propto p(T + m_e)|\mathcal{M}|^2 F(T) K^2(T)\,,$$

where

$$K(T) \approx (Q-T)\left[1 - \frac{m_\beta^2}{(Q-T)^2}\right]^{1/4}.$$

The Curie diagram (Fig. 7a) for the allowed processes is a sensitive test of the effective neutrino mass m_β.

Figure 7b shows the published results on m_β^2 obtained from tritium decays since 1990. In experiments carried out in Los Alamos, Zurich, Tokyo, Beijing, and Livermore, magnetic spectrometers were used, and in experiments carried out in Troitsk and Mainz, electrostatic filters with magnetic adiabatic collimators were utilized. At present, the most precise result is obtained from the Troitsk experiment [42]:

$$m_\beta^2 = (-0.67 \pm 1.89(\text{stat.}) \pm 1.68(\text{syst.}))\ \text{eV}^2\,,$$

which implies the bound $m_{\nu_e} < 2.2$ eV at a 95% CL. The Mainz group established a comparable bound: $m_{\nu_e} < 2.4$ eV at a 95% CL. We note that the upper bound can be somewhat changed depending on the method used in the analysis. For example, the analysis of the Troitsk data using the Feldman–Cousins method yields a somewhat stronger bound: $m_{\nu_e} < 2.05$ eV at the 95% CL [42].

The KATRIN (Karlsruhe Tritium Neutrino) experiment is a next-generation experiment with a sensitivity of 0.2 eV to the neutrino mass [70]. Here, if the neutrino mass turns out to be different from zero, it can be measured quite precisely: the measurement accuracy will be 5σ for $m_\nu = 0.35$ eV or 3σ for $m_\nu = 0.3$ eV. The spectrometer of the detector is completely mounted, and the source and the transport section will be installed by the summer of 2016; then test runs at a small density will begin. The data taking is assumed to start in 2017.

2.2 Mass hierarchy and CP-invariance violation

2.2.1 Neutrino mass hierarchy. We briefly discuss the prospects of determining the mass hierarchy by different approaches. In the literature, the statement can be found that the neutrino mass hierarchy is determined just by the sign of Δm_{31}^2. This is only partially true. More correctly, for different neutrino mass hierarchies, both the sign and absolute value of Δm_{31}^2 vary.

We use the superscripts N and I to denote the neutrino masses for the normal, $m_1^N < m_2^N < m_3^N$, and inverted, $m_3^I < m_1^I < m_2^I$, hierarchies. Thus, we have two sets of parameters Δm_{ij}^2: $\Delta m_{21}^{2,N}$, $\Delta m_{31}^{2,N}$, $\Delta m_{32}^{2,N}$ and $\Delta m_{21}^{2,I}$, $\Delta m_{31}^{2,I}$, $\Delta m_{32}^{2,I}$. Only two differences of the mass squares Δm_{ij}^2 are

linearly independent, because

$$\Delta m^2_{31} = \Delta m^2_{32} + \Delta m^2_{21}\,. \tag{14}$$

The mass hierarchy is defined as follows:

$$\begin{aligned} &\text{N:}\quad \Delta m^2_{31} \geqslant 0\,,\ \Delta m^2_{32} \geqslant 0\,,\ |\Delta m^2_{31}| = |\Delta m^2_{32}| + \Delta m^2_{21}\,,\\ &\text{I:}\quad \Delta m^2_{31} \leqslant 0\,,\ \Delta m^2_{32} \leqslant 0\,,\ |\Delta m^2_{31}| = |\Delta m^2_{32}| - \Delta m^2_{21}\,. \end{aligned} \tag{15}$$

The vacuum oscillation probability depends on the neutrino mass ordering. For example, the electron neutrino survival probability P_{ee} is expressed as

$$\begin{aligned} 1 - P_{ee} = {}& \cos^4\theta_{13}\sin^2(2\theta_{12})\sin^2\Delta_{21} + \sin^2(2\theta_{13})\\ &\times(\cos^2\theta_{12}\sin^2\Delta_{31} + \sin^2\theta_{12}\sin^2\Delta_{32})\,, \end{aligned} \tag{16}$$

where $\Delta_{ij} \equiv \Delta m^2_{ij} L/(4E_\nu)$.

A different neutrino mass ordering leads to a different survival probability:

$$\begin{aligned} P^{\mathrm{N}}_{ee} - P^{\mathrm{I}}_{ee} = {}& -\sin^2(2\theta_{13})\big[\cos^2\theta_{12}(\sin^2\Delta^{\mathrm{N}}_{31} - \sin^2\Delta^{\mathrm{I}}_{31})\\ &+ \sin^2\theta_{12}(\sin^2\Delta^{\mathrm{N}}_{32} - \sin^2\Delta^{\mathrm{I}}_{32})\big]\,. \end{aligned} \tag{17}$$

Equation (17) implies that if the neutrino mass hierarchy were defined only by the signs of Δm^2_{31} and Δm^2_{32}, the difference $P^{\mathrm{N}}_{ee} - P^{\mathrm{I}}_{ee}$ would be identically zero. Because both Δm^2_{31} and Δm^2_{32} vary with changing the hierarchy, $P^{\mathrm{N}}_{ee} - P^{\mathrm{I}}_{ee} \neq 0$ in general. This is the key observation in determining the hierarchy in experiments with reactor antineutrinos. The optimal distance between the detector and reactor, which is most sensitive to the mass hierarchy determination, is 52–53 km [71].

Two experiments, JUNO (Jiangmen Underground Neutrino Observatory) [72] and RENO-50 (Reactor Experiment for Neutrino Oscillations 50) [73], plan to measure the neutrino mass hierarchy using reactor antineutrinos. The JUNO experiment, in which physicists from JINR are actively participating, will use a 20 kt LS detector watched from inside by 20,000 PMTs. The spectrum of reactor antineutrinos is modulated by neutrino oscillations with frequencies defined by $\Delta m^2_{21} L/E_\nu$ and $\Delta m^2_{31} L/E_\nu$ and depends on the neutrino mass hierarchy. The mass hierarchy can be measured only with a detector that has good energy resolution, better than 3% for one MeV of released energy. The JUNO collaboration hopes to reach the required energy resolution.

Physicists from JINR are also actively participating in experiments with accelerator neutrinos aimed at measuring the neutrino mass hierarchy. Experiments with accelerator neutrinos NOvA (NuMi (Neutrino at Main Injector) Off-axis ν_e Appearance) [74] (at the stage of data collecting) and DUNE (Deep Underground Neutrino Experiment)[5] (at the stage of preparation) [75] use neutrino and antineutrino oscillations in matter to determine the neutrino mass hierarchy. These experiments observe the appearance of electron neutrinos (antineutrinos) in a muon neutrino (antineutrino) beam at a large distance from the source. Because most of the neutrino path lies under the ground, the transition probability of neutrinos with a certain energy is modified by matter. Qualitatively, the effect of matter can be viewed as follows. Electron neutrinos in matter become 'heavier', and at the exit from matter occur with a higher probability in the respective state ν_τ or ν_μ in the case of the normal or inverted mass hierarchy.

[5] The former LBNE (Long Baseline Neutrino Experiment).

Table 2. Schematic chain of transitions from initial flavor states to eigenstates in matter ν_i^{m} and next to flavor final states for normal and inverted hierarchy.

Normal hierarchy	Inverted hierarchy
$\nu_e \to \nu_3^{\mathrm{m}} \to \nu_\tau$	$\nu_e \to \nu_2^{\mathrm{m}} \to \nu_\mu$
$\nu_\tau \to \nu_2^{\mathrm{m}} \to \nu_\mu$	$\nu_\mu \to \nu_1^{\mathrm{m}} \to \nu_\tau$
$\nu_\mu \to \nu_1^{\mathrm{m}} \to \nu_e$	$\nu_\tau \to \nu_3^{\mathrm{m}} \to \nu_e$

The corresponding neutrino transitions from a certain initial flavor ν_α to eigenstates ν_i^{m} in matter and later into a certain final flavor ν_β are presented in Table 2. As a result, due to the matter effect, the oscillation probability $P_{\mu e}$ respectively increases or decreases for the normal and inverted hierarchy, which leads to a different number of registered ν_μ and ν_e events in the experiment.

The modification of neutrino oscillations in matter will be used in atmospheric neutrino experiments PINGU (Precision IceCUbe Next Generation Upgrade) [76], Hyper-Kamiokande [78], and INO (India-based Neutrino Observatory) [79]. Because both muon and electron neutrinos are produced in the atmosphere, such experiments are sensitive to four oscillation channels simultaneously: $\nu_\mu \to \nu_\mu$, $\nu_\mu \to \nu_e$, $\nu_e \to \nu_e$, $\nu_e \to \nu_\mu$ for both neutrinos and antineutrinos. In addition, these experiments are sensitive to neutrinos coming at different incidence angles, which correspond to different path lengths inside the earth. In the case of the normal hierarchy, the survival probability of atmospheric muon neutrinos passing through Earth has a resonance at the energy of 5 GeV and the zenith angle $\cos\theta = -0.95$, unlike the survival probability of muon antineutrinos. The other three channels show more pronounced oscillations for neutrinos than for antineutrinos. In the case of the inverted hierarchy, the behavior is different: antineutrinos have more pronounced transition probabilities than neutrinos. Although atmospheric neutrino experiments, as a rule, cannot distinguish neutrinos and antineutrinos, the hierarchy determination in these experiments is possible by taking differences in the flux, cross section, and kinematics of neutrinos (antineutrinos) into account.

Cosmological measurements are also sensitive to the neutrino mass hierarchy. In the case of a normal mass hierarchy, the sum $\sum_i m_i$ is mainly determined by the heaviest mass, m_3, because $|\Delta m^2_{31}| \gg \Delta m^2_{21}$ and $\sum_i m_i \simeq m_3 \geqslant 0.05$ eV. The inverted hierarchy assumes that $m_3 \ll m_{1,2}$, and then $\sum_i m_i \simeq (m_1 + m_2) \geqslant 0.1$ eV. The precision of cosmological measurements should be improved 2–4-fold relative to the present-day accuracy to reach sufficient sensitivity to the neutrino mass hierarchy. The next generation of the galaxy cluster catalogs will be quite sensitive to the neutrino mass scale, which will enable the study of both neutrino mass hierarchies.

The effective neutrino mass $m_{\beta\beta}$ obtained from the neutrinoless double beta decay probability depends on the neutrino mass hierarchy, which is discussed in Section 2.3. Thus, searching for $0\nu\beta\beta$ decays is an additional source of information on the neutrino mass hierarchy.

Estimates of the sensitivity of some experiments [80] are presented in Fig. 8. Current and future experiments on the

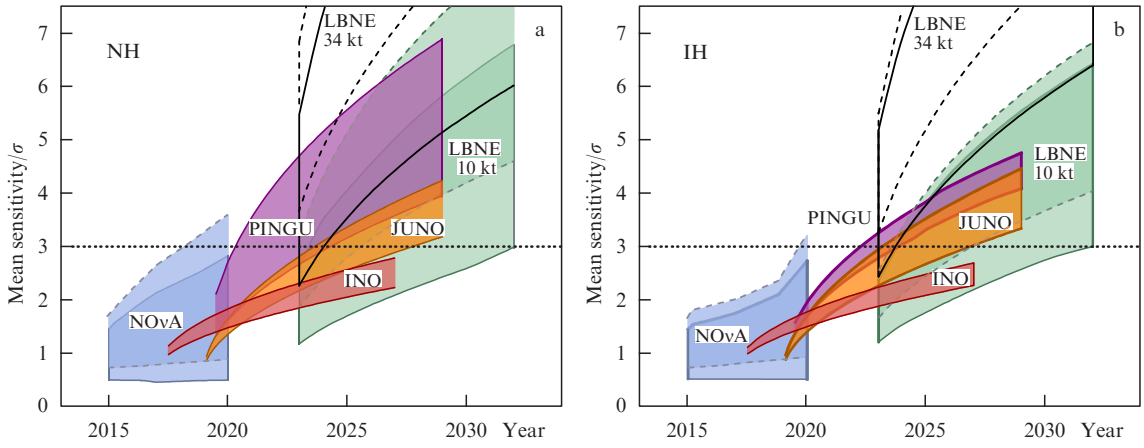

Figure 8. Comparative sensitivity estimate (σ is the standard deviation) of neutrino experiments depending on the mass hierarchy (NH or IH) realized in Nature [80]. For long-baseline experiments, regions inside solid (dashed) contours correspond to the true value $\theta_{23} = 40^\circ$ ($\theta_{23} = 50^\circ$).

neutrino mass hierarchy determination are complementary from the standpoint of both the time of the data taking and sensitivity, and the data taking time and physical methods used. Clearly, reaching high statistical significance is a fairly complicated problem, especially if the inverted mass hierarchy is realized in nature. To reliably determine the neutrino mass hierarchy, a joint analysis of different experimental data will possibly be required.

2.2.2 CP-invariance violation. Violation of CP invariance shows up in the asymmetry of neutrino and antineutrino oscillations:

$$\mathcal{A}_{\rm CP} = \frac{P(\nu_\mu \to \nu_e) - P(\bar\nu_\mu \to \bar\nu_e)}{P(\nu_\mu \to \nu_e) + P(\bar\nu_\mu \to \bar\nu_e)}\,.$$

In the three-neutrino model, this asymmetry can be represented in the leading order in Δm^2_{21} as

$$\mathcal{A}_{\rm CP} \sim \frac{\cos\theta_{23}\sin(2\theta_{12})\sin\delta}{\sin\theta_{23}\sin\theta_{13}}\left(\frac{\Delta m^2_{21}L}{4E_\nu}\right) + \ldots, \qquad (18)$$

where the ellipsis denotes terms describing the interaction of neutrinos (antineutrinos) with matter.

A nonzero value of the mixing angle θ_{13} opens prospects to measure the phase δ related to CP-parity violation in the lepton sector. Among the presently running experiments, only NOνA and T2K (Tokai to Kamioka) are somewhat sensitive to the CP-invariance breaking.

Figures 9 and 10 show the probabilities of $\nu_\mu \to \nu_e$ and $\bar\nu_\mu \to \bar\nu_e$ oscillations as a function of energy and the neutrino propagation path length for normal and inverted hierarchies. It is seen that precise measurements of such neutrino oscillograms will enable determination of the neutrino mass hierarchy and the parameter δ. These measurements will be carried out by the DUNE experiment [81], which will be performed with two detectors separated by 1300 km (a time-projection camera with liquid argon). The first results are expected in 2025–2030.

2.3 Neutrinoless double beta decay

The idea of an 'ordinary' double beta decay was put forward by Marie Goeppert-Meyer. In 1935, she was the first to consider the process $(A, Z) \to (A, Z+2) + 2e^- + 2\bar\nu_e$ [82], in which, in addition to two electrons, two antineutrinos are emitted, and the lepton number is conserved ($\Delta L = 0$). This process, which is two consecutive nuclear β-decays with intermediate states, is allowed in the SM independently of the nature of the neutrino.

In 1937, Majorana showed that no results of the theory of beta decay change if the neutrino is identical to its own antiparticle (a Majorana particle) [83]. In 1939, Furry, based on Majorana's paper, showed that if the neutrino is a Majorana particle, neutrinoless double beta decay ($0\nu\beta\beta$) is possible: $(A, Z) \to (A, Z+2) + 2e^-$ [84].

This process is much more interesting, because the lepton charge changes by two units ($\Delta L = 2$): two electrons are ejected by a nucleus without neutrino emission. The neutrinoless double beta decay is forbidden in the SM if the neutrino is a Dirac fermion.

To make the $0\nu\beta\beta$ decay possible, two neutrons (from the same nucleus) must be exchanged by a virtual neutrino state and, simultaneously, the neutrino must be identical to the antineutrino, i.e., it should be a Majorana fermion. This is a necessary but not sufficient condition for the $0\nu\beta\beta$ decay. It is also necessary that the neutrino have a nonzero mass, because otherwise the neutrino emitted by the first neutron would have the right helicity, while the second neutron can absorb only a neutrino with the left helicity. The nonzero mass of the Majorana neutrino makes the $0\nu\beta\beta$ decay possible with the probability amplitude proportional to the effective neutrino mass:

$$A \propto m_{\beta\beta} = \sum_i V^2_{ei} m_i\,.$$

A monoenergetic peak at the decay energy Q is the 'signature' of $0\nu\beta\beta$ decay.

One of the most sensitive experiments, Heidelberg–Moscow (HdM), searched for the $0\nu\beta\beta$-decay $^{76}\mathrm{Ge} \to {}^{76}\mathrm{Se} + 2e^-$ for 10 years using the enriched isotope ^{76}Ge ($Q_{\beta\beta} = 2039.061 \pm 0.007$ keV).

In 2001, the leader of the HdM collaboration G V Klapdor-Kleingrothaus and colleagues claimed the observation of $0\nu\beta\beta$ decay with the lifetime $T_{1/2} = 1.5 \times 10^{25}$ years [85]. In 2004, using a final analysis of all data obtained, the effective neutrino mass was reported to be $\langle m_{\beta\beta}\rangle = 0.24 - 0.58$ eV [86]. However, this result was criticized in [87, 88], and it became clear that it has to be reconfirmed using more sensitive experiments.

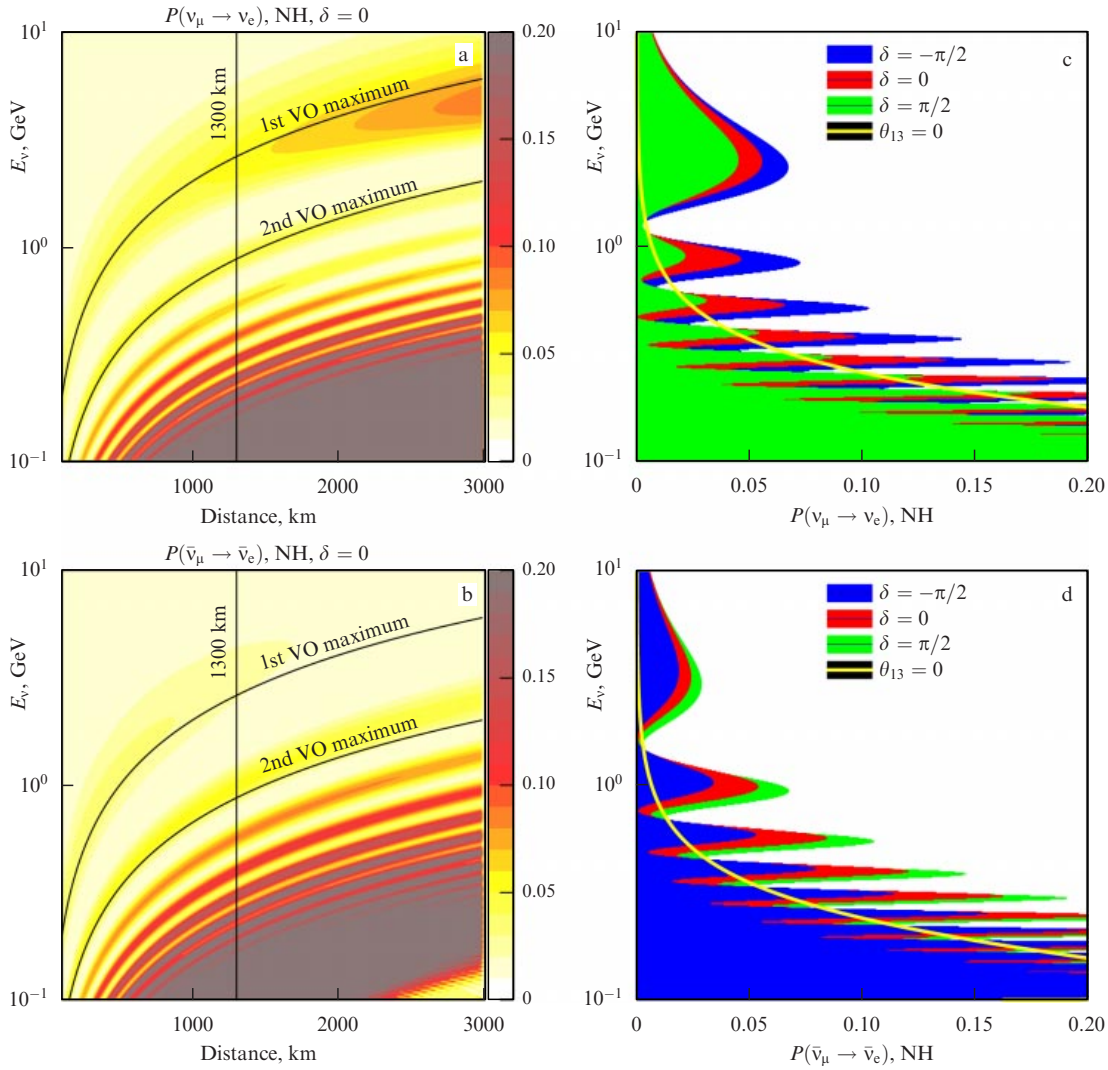

Figure 9. (Color online.) Probability of oscillations (a) $\nu_\mu \to \nu_e$ and (b) $\bar\nu_\mu \to \bar\nu_e$ as a function of energy and the neutrino path length for the normal hierarchy (NH) assuming $\delta = 0$ (VO are vacuum oscillations). Probability of oscillations (c) $\nu_\mu \to \nu_e$ and (d) $\bar\nu_\mu \to \bar\nu_e$ as a function of energy for $L = 1300$ km and three values of δ $(-\pi/2, 0, \pi/2)$. The yellow line corresponds to the probability of the appearance of electron neutrinos only due to the mixing of ν_1 and ν_2. (From Ref. [81].)

First of all, it is necessary to perform a more precise experiment using the same ^{76}Ge isotope to avoid uncertainties induced by the structure of another nucleus. In 2014, the GERDA (Germanium Detector Array) experiment [89], using detectors with ^{76}Ge, set the bound $T^{0\nu}_{1/2} > 2.1 \times 10^{25}$ years with an exposure of 21.6 kg year. Searches with the ^{136}Xe nucleus by the KamLand-Zen [47] and EXO-200 [48] collaborations have not found double neutrinoless beta decays of this nucleus either, and set the lower lifetime bound $T^{0\nu}_{1/2} > 2.6 \times 10^{25}$ years. This also contradicts the results in [85, 86].

The effective mass $|m_{\beta\beta}|$ obtained from the $0\nu\beta\beta$ decay as a function of the mass of the lightest neutrino for the normal and inverted mass hierarchies is presented in Fig. 11. Next-generation experiments will be sensitive to the Majorana nature of the neutrino for the inverted hierarchy. For the normal mass hierarchy, the sensitivity should be increased by an order of magnitude. Nondetection of the $0\nu\beta\beta$ decay for the normal mass hierarchy will strongly suggest the Dirac nature of the neutrino.

We note that, according to the Schechter–Valle theorem [91], if neutrinoless double beta decay is observed, then, irrespective of the nature of the $0\nu\beta\beta$ process itself, at least one of the known neutrinos is a Majorana particle with a nonzero mass.

2.4 Sterile neutrinos

There are several anomalous results in neutrino physics whose explanation in terms of neutrino oscillations requires the introduction of a sterile neutrino.

The LSND collaboration discovered an excess of $\bar\nu_e$ at a distance of 30 m from decaying charged muons at rest, $\mu^+ \to e^+ + \nu_e + \bar\nu_\mu$ [92]. This result can be interpreted as oscillations $\bar\nu_\mu \to \bar\nu_e$ with $\Delta m^2 \simeq 1$ eV^2. The mean energy of $\bar\nu_e$ is $\langle E_\nu \rangle = 30$ MeV.

One of the main goals of the MiniBooNE (BooNE — Booster Neutrino Experiment) collaboration was to check the LSND result by changing the distance between the source and the detector and the energy of neutrinos while keeping the same ratio $L/E_\nu \simeq 500\,\text{m}/500\,\text{MeV}$ as in LSND. MiniBooNE, unlike LSND, is capable of registering both antineutrinos and neutrinos. The data were collected in 2002–2012 in the neutrino and antineutrino modes.

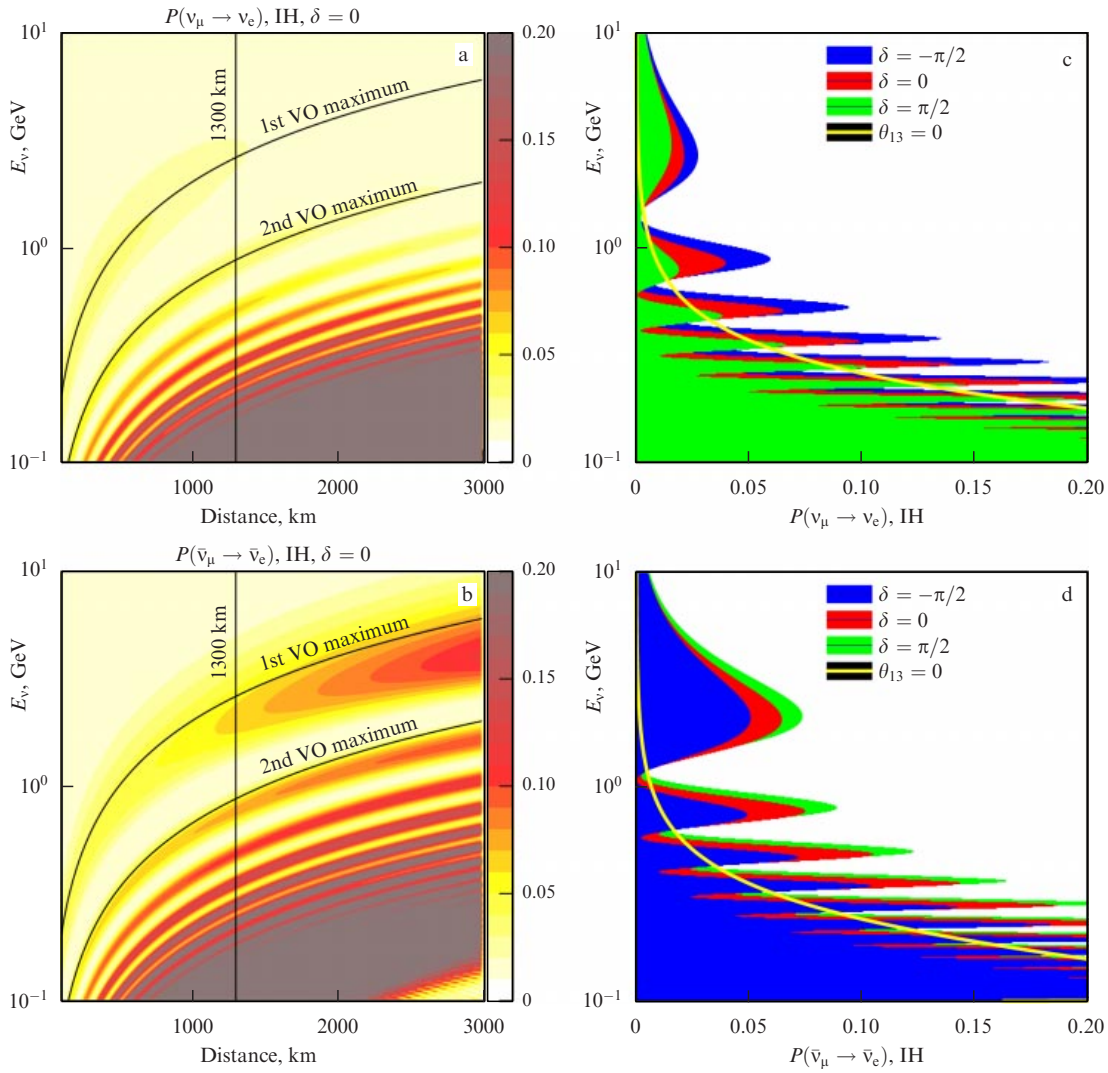

Figure 10. (Color online.) Probability of oscillations (a) $\nu_\mu \to \nu_e$ and (b) $\bar\nu_\mu \to \bar\nu_e$ as a function of energy and the neutrino path length for the inverted hierarchy (IH) assuming $\delta = 0$ (VO are vacuum oscillations). Probability of oscillations (c) $\nu_\mu \to \nu_e$ and (d) $\bar\nu_\mu \to \bar\nu_e$ as a function of energy for $L = 1300$ km and three values of δ $(-\pi/2, 0, \pi/2)$. The yellow line corresponds to the probability of the appearance of electron neutrinos only due to the mixing of ν_1 and ν_2. (From Ref. [81].)

The MiniBooNE experiment results [93] are as follows: in the antineutrino mode, an excess of $\bar\nu_e$ events of 78.4 ± 28.5 (2.8σ) in the energy range $200 < E_\nu^{QE} < 1250$ MeV is observed, which is compatible with neutrino oscillations with $0.01 < \Delta m^2 < 1$ eV^2 and is partially compatible with the LSND results; in the neutrino mode, an excess of ν_e events of 162.0 ± 47.8 (3.4σ) is also observed, but the form of energy distribution of these events only minimally agrees with the simple two-neutrino oscillation formalism. If the oscillation formalism is extended by including several sterile neutrinos and the CP-invariance is violated, it is possible to diminish the disagreement between the neutrino and antineutrino modes. Thus, the MiniBooNE results have not clarified the LSND anomaly.

The SAGE (Soviet–American Gallium Experiment) radio-chemical gallium solar detectors [94, 95] and, independently, GALLEX (Gallium Experiment) [96, 97] performed measurements with artificial sources of neutrinos. Two types of radioactive sources were used: those based on ^{51}Cr (electron capture, neutrino energy of 752.7 keV) and on ^{37}Ar (electron capture, neutrino energy of 813.5 keV). Both experiments discovered a deficit of observed neutrinos compared to the expected value. The joint mean ratio of the observed counting rates to the expectation value is 0.87 ± 0.05. The interpretation of this result by neutrino oscillations requires that $\Delta m^2 > 0.1$ eV^2.

Another anomaly is the so-called reactor anomaly. This term appeared in 2011 after the publication of paper [98], in which new calculations of reactor antineutrino spectra for ^{235}U, ^{239}Pu, ^{241}Pu, and ^{238}U were presented. The reassessment of the spectra resulted in a 3% increase in the expected antineutrino fluxes; in good approximation, this estimate is valid for all reactor experiments performed earlier. The joint analysis of all published experimental data for distances less than 100 m yields the observed to expected flux ratio 0.943 ± 0.023, i.e., the deviation from unity has a statistical significance of 98.6%.

To be explained by neutrino oscillations, all results discussed above require that $\Delta m^2 \simeq 0.01 - 1$ eV^2, which is incompatible with the three-neutrino oscillation framework, which has only two independent quantities, Δm^2_{21} and Δm^2_{31}, whose measured values are much smaller. A straightforward increase in the number of the neutrino types to four or more is also impossible, because this would contradict the observed

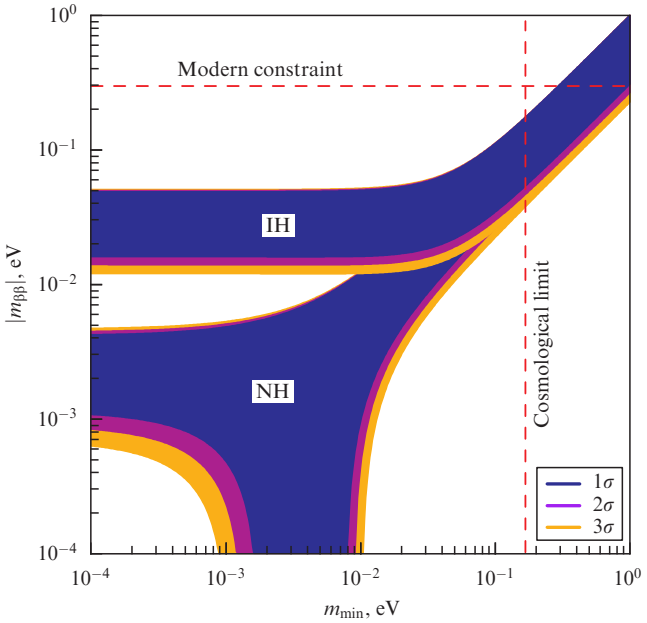

Figure 11. Effective mass $|m_{\beta\beta}|$ as a function of the lightest neutrino mass for the normal (NH) ($m_{\min} = m_1$) and inverted (IH) ($m_{\min} = m_3$) neutrino mass hierarchies from the Daya Bay experiment [90].

Z^0-boson width, which agrees with three neutrino generations with the masses less than $m_Z/2$ in the SM framework. To bring the discussed anomalies into agreement with the observed Z^0-boson width, the so-called *sterile* neutrino can be introduced.

The sterile neutrino is a superposition of four (or more) massive neutrinos, which, as a whole, does not interact with $W^\pm$ and Z^0; however, each of the massive neutrinos interacts with $W^\pm$ and Z^0 bosons. How can these apparently contradicting conditions be reconciled? For this, additional neutrinos are introduced into the SM without introducing new charged leptons. We illustrate this idea by restricting ourselves to only one such additional neutrino. Four neutrino combinations arise, which are superpositions of all four massive states:

$$\begin{pmatrix} \nu_\alpha \\ \nu_s \end{pmatrix} = \begin{pmatrix} V_{3\times3} & K_{3\times1} \\ U_{1\times3} & M_{1\times1} \end{pmatrix} \begin{pmatrix} \nu_m \\ \nu_4 \end{pmatrix},$$

where $V_{3\times3}$ is the usual 3×3 leptonic mixing matrix and $K_{3\times1}$, $U_{1\times3}$, and $M_{1\times1}$ are additional matrix blocks of a new unitary 4×4 mixing matrix, with $\nu_m = (\nu_1, \nu_2, \nu_3)$. The unitarity conditions of the new 4×4 mixing matrix are

$$V^\dagger V + U^\dagger U = 1_{3\times3}\,,\quad K^\dagger K + M^\dagger M = 1_{1\times1}\,,\quad V^\dagger K + U^\dagger M = 0_{3\times1}\,,$$
$$V^\dagger V + K^\dagger K = 1_{3\times3}\,,\quad U^\dagger U + M^\dagger M = 1_{1\times1}\,,\quad VU^\dagger + KM^\dagger = 0_{3\times1}\,. \tag{19}$$

A neutrino state with a certain flavor $\nu_\alpha = \sum_i V_{\alpha i}\nu_i + K_{\alpha1}\nu_4$ includes ν_4. The combination of states $\nu_s = \sum_i U_{1i}\nu_i + M_{11}\nu_4$, which has no corresponding charged lepton, turns out to be singular: the amplitude of production of the charged lepton ℓ_α by the state ν_s is zero with good accuracy (although not identically):

$$\mathcal{A}(\nu_s + W^- \to \ell_\alpha^-) = \sum_{i=1}^{3} U_{1i}V^\dagger_{i\alpha}\mathcal{A}_i + M_{11}K^\dagger_{1\alpha}\mathcal{A}_4$$
$$\simeq (UV^\dagger + MK^\dagger)_{1\alpha}\mathcal{A}_0 = 0\,,$$

where we used unitarity condition (19), $\mathcal{A}_i$ and $\mathcal{A}_4$ are the production amplitudes that are independent of the flavor but depend on the neutrino mass, and $\mathcal{A}_0$ is the corresponding amplitude in the case of a negligibly small neutrino mass. We stress that the amplitude $\mathcal{A}(\nu_s + W^- \to \ell_\alpha^-)$ vanishes in the approximation of a negligibly small neutrino mass and only for the coherent addition of all contributions from massive neutrinos. The last condition can be violated for sufficiently large neutrino mass differences, as is the case with suppressed oscillations of charged leptons (see Section 1.3). The sterile neutrino ν_s, being a noncoherent mixture of massive states, then interacts with $W^\pm$, Z^0, and charged leptons ℓ_α.

It is also easy to show that the partial widths of $W^\pm$ and Z^0 boson decays with a neutrino or antineutrino in the final state are proportional to the number of neutrino species, which is three and not four, although each massive neutrino interacts with gauge bosons.[6] How can the additional neutrinos be discovered?

First of all, in the plasma of the early Universe, the fourth massive neutrino should show up as an additional relativistic degree of freedom, to which cosmological and astrophysical observations are sensitive. Second, active flavor combinations of four fields ν_α in the course of the time evolution of a state can acquire a nonzero contribution of the sterile combination ν_s, which can result in a periodic disappearance of the flavor α, and this could be discovered in sufficiently short-distance experiments. Third, additional neutrino species contribute to the effective neutrino masses in particle decays. Finally, we note that the matrix $V_{3\times3}$ should be nonunitary in this scenario, which could be discovered by precisely measuring all of its elements.

Presently, a large number of projects on searching for short-distance oscillations are under discussion [99]. In the SOX (Short distance neutrino Oscillations with BoreXino) project [100], it is proposed to use the Borexino detector, which is capable of precisely reconstructing the energy and the interaction point. In 2016–2017, an experiment with a ^{144}Ce source of antineutrinos will be carried out. The detector size and spatial resolution enable registering the oscillation pattern for oscillations with $\Delta m^2 \sim 1$ eV^2.

The BEST (Baksan Experiment of Sterile Transitions) project at the Baksan Laboratory is designed to use a monoenergetic neutrino source based on the ^{51}Cr isotope [101]. Neutrinos will be detected by gallium from the SAGE experiment, which will be placed around the source in two zones at different mean distances from the source. This experiment will be sensitive at the level of several percent to the disappearance of electron neutrinos and will be able to search for transitions of active neutrinos to sterile states for the oscillation parameters $\Delta m^2 > 0.5$ eV^2 and $\sin^2(2\theta) > 0.1$.

The search for short-distance oscillations is also possible near nuclear reactors. Preferably, the size of the active zone of the reactor would be much smaller than the oscillation length. The PIK research reactor in Gatchina (active zone height is 50 cm, diameter is 39 cm [102]) and the research reactor in Dimitrovgrad (the zone size is $42\times42\times35$ cm^3 [103]) are suitable for this study. Oscillations can be sought with liquid

[6] We note that another definition of the sterile neutrino can be found in the literature. For example, sterile neutrinos are sometimes referred to as 'seed' states that do not interact with $W^\pm$ and Z^0 bosons and have no certain mass but are mixed with the 'seed' massless flavor neutrinos in Yukawa interactions.

Table 3. Prediction of the standard solar model and experimental measurements of solar neutrino fluxes.

ν flux	Model GS98 [114]	Model AGS09 [115]	$cm^{-2}\ s^{-1}$	Measured value, experiment*
pp	5.98 ± 0.04	6.03 ± 0.04	$\times 10^{10}$	6.0 ± 0.8, SAGE + SNO + Homestake [108] 6.6 ± 0.7, Borexino [109] 6.37 ± 0.46, all solar
pep	1.44 ± 0.012	1.47 ± 0.012	$\times 10^{8}$	1.6 ± 0.3, Borexino [110]
^{7}Be	5.00 ± 0.07	4.56 ± 0.07	$\times 10^{9}$	4.87 ± 0.24, Borexino [111]
^{8}B	5.58 ± 0.14	4.59 ± 0.14	$\times 10^{6}$	5.2 ± 0.3, SNO + SK + Borexino + KamLAND $5.25 \pm 0.16^{+0.011}_{-0.013}$, SNO – LETA [112]
hep	8.0 ± 2.4	8.3 ± 2.5	$\times 10^{3}$	$< 2.3 \times 10^{4}$ $cm^{-2}\ s^{-1}$ (90% CL), SNO [113]
^{13}N	2.96 ± 0.14	2.17 ± 0.14	$\times 10^{8}$	Integral CNO flux: < 7.4 Borexino (90% CL) [110]
^{15}O	2.23 ± 0.15	1.56 ± 0.15	$\times 10^{8}$	
^{17}F	5.52 ± 0.17	3.40 ± 0.16	$\times 10^{6}$	
* SK — Super-KamiokaNDE, LETA — Low Energy Threshold Analysis.				

scintillator (LS) detector of a relatively small volume; for example, in the Poseidon experiment [104], an LS detector with the central zone size of $1 \times 1 \times 1.5$ m^3 is planned to be placed at a distance of 5–15 m from a 100 MW reactor. The sensitivity of such a detector to the oscillation parameters falls within the range $\Delta m^2 = 0.3-6$ eV^2 and $\sin^2(2\theta) > 0.01$.

The DANSS (Detector of Anti-Neutrino based on Solid Scintillator) experiment was proposed by a group of researchers from JINR and ITEP to be carried out at the Kalinin NPP [105, 106]. For the first time, a solid scintillator will be used to detect reactor antineutrinos. The new-generation DANSS antineutrino detector will include a plastic scintillator with a volume of 1 m^3 divided into 2500 cells and 10 autonomous sections, each with 250 cells. The count rate of antineutrinos will be about 10,000 events a day at a distance of 11 m from the reactor, which corresponds to a 1% statistical accuracy of measurements. Besides other tasks, the DANSS spectrometer is planned to be used for sterile neutrino searches. An important feature of the DANSS experiment is the variable distance between the reactor center and the detector within the range from 9.7 m to 12.2 m.

Another Russian project is the Neutrino-4 experiment [107] with variable distance as in the DANSS project but with the use of a research reactor with a power up to 100 MW.

The unitarity of the mixing matrix can be tested in the next-generation experiments, such as JUNO and DUNE, in which the mixing parameters will be measured with an accuracy of better than 1%, i.e., more precisely than in the quark sector.

2.5 Solar metallicity problem and the CNO cycle

The detection of solar neutrinos not only confirmed the theory of nuclear reactions in the Sun, but also revolutionized particle physics by showing that neutrinos oscillate and are therefore massive particles. But the full theory of nuclear reactions in stars has not been completely confirmed yet. The theory assumes that energy in stars is generated in two main chains of nuclear reactions in which helium is synthesized: in the proton–proton chain, which is the main energy source for stars of the solar mass and below, and in the carbon–nitrogen–oxygen cycle (CNO), which dominates in more massive stars, and thus is the main source of hydrogen depletion in the Universe. The CNO reactions make a minor contribution to the total power of the Sun; nevertheless, this energy flux can be registered at the present-day sensitivity of neutrino detectors.

According to modern views, more massive stars with higher central temperatures are powered by the CNO cycle. The model of energy generation in more massive stars has not so far been checked experimentally. Neutrinos from distant massive stars cannot be detected on Earth due to extremely low fluxes, but the CNO neutrinos from the Sun can be registered. Experimental detection of these neutrinos would test theoretical ideas on the energy generation mechanism in massive stars.

Table 3 presents the results of measurements of solar neutrino fluxes in comparison with theoretical predictions in the standard solar model (SSM) in two variants (GS98 and AGS09), which correspond to different methods of determining heavy elemental abundance in the Sun, or metallicity.[7] The abundance of chemical elements on the solar surface was calculated more than 10 years ago in a one-dimensional model (the static model GS98 [114] for separate layers of the solar atmosphere, the photosphere and chromospheres), using spectroscopic observations of the solar photosphere. This model is in agreement with helioseismological observations that measure the change in the propagation velocity of mechanical waves in the Sun.

The situation changed in 2007 when the Asplund group published the results of calculations of solar chemical abundance using a 3D magnetohydrodynamic model (AGS09) of the convective zone, photosphere, and corona. In the AGS09 model, the abundance of elements such as C, N, and O is significantly lower than in the GS98 model. The solar metallicity in general was reduced to $Z/X = 0.0178$ (low metallicity), while the previous value was $Z/X = 0.0229$ (high metallicity). The 3D model reproduces observed profiles of atomic and molecular lines in the solar photosphere, but contradicts helioseismological data. This disagreement has not yet been satisfactorily resolved [116].

Solar CNO neutrino fluxes are relatively low and have not been directly measured so far. Only integral measurements of the total neutrino fluxes in two radiochemical experiments have been carried out.

[7] In astrophysics, metallicity is the relative concentration of elements heavier than helium. The mass ratio Z/X of elements heavier than helium (Z) to the mass of hydrogen (X) is typically used.

Measurements of CNO neutrino fluxes are included in the program of the second phase of the Borexino experiment and the solar phase program of the SNO+ experiment [117].

2.6 Astrophysical neutrinos and neutrino telescopes

On 23 February 1987, a supernova exploded in the Large Magellanic Cloud at a distance of 51.4 kpc from the Sun. According to the modern theory, around 10^{58} neutrinos should be emitted during a supernova explosion. Almost 99% of the explosion energy, about 10^{46} J, is carried away by neutrinos and antineutrinos.

Three experiments, Kamiokande II [118], IMB (Irvine–Michigan–Brookhaven) [119] and BUST (Baksan Underground Scintillation Telescope) [120], detected neutrinos from the 1987 supernova explosion two hours before the appearance of the optical signal, in correspondence with the theory of the supernova mechanism. The Soviet–Italian neutrino telescope LSD (Liquid Scintillation Detector) under Mont Blanc registered five neutrino events [121, 122], but 7.5 h before the appearance of the optical signal. The background fluctuations in this detector can imitate such an event sequence only once in three years [123]. The probability of the coincidence of the neutrino signal with the optical signal from the supernova within 24 h decreases the probability of a background fluctuation by 365 times, i.e., such an event can occur accidentally only once every 1000 years [123]. Usually, the LSD data are ignored in the analysis, although the LSD observations can evidence the two-stage character of the neutrino emission. The possible mechanism was discussed, for example, in paper [124].

For the early detection of supernovae, a devoted network SNEWS (Super Nova Early Warning System) [125] was set. The network integrate active detectors sensitive to supernova neutrinos: LVD (Large Volume Detector), Super-Kamiokande, AMANDA (Antarctic Muon And Neutrino Detector Array)/Ice Cube, Borexino, KamLAND, and Daya Bay; The SNO+ detector will join the network after the beginning of operation. The triangulation of neutrino signals allows determination of the direction to the supernova, which opens the possibility of observing the supernova explosion development in the optical spectrum (neutrinos are emitted before the electromagnetic outburst).

New generation detectors, such as Hyper-Kamiokande, JUNO, RENO-50, and LENA (Low Energy Neutrino Astrophysics), with a target mass from 20 to 400 kt, are expected to detect the number of events from a supernova explosion 2–3 orders of magnitude higher than with first-generation detectors.

In 2013, the IceCube collaboration [126] reported the detection of three events with energies of 1.0, 1.1, and 2.2 PeV. These events are interpreted as astrophysical neutrinos. This is a revolutionary result, indicating the birth of a new branch of science — neutrino astronomy — right in front of our eyes.

In comparing the observed energy spectrum with the expected one, by assuming the existence of only atmospheric neutrinos and muons, the Ice Cube collaboration concluded that there are additional 87^{+14}_{-10} neutrinos that can come from astrophysical objects [127]. However, the source of these neutrinos remains a puzzle.

The low angular resolution of shower events in the ice on the South Pole precludes the determination of possible sources of the observed events. Detection of astrophysical sources of neutrinos is the main goal of the Baikal-GVD (Gigaton Volume Detector) project, KM3NET (Cubic Kilometer Neutrino Telescope) [128], ANTARES (Astronomy with a Neutrino Telescope and Abyss environmental RESearch project) [129], and IceCube.

The revolutionary discovery of astrophysical neutrinos by the IceCube collaboration provided a huge impetus to development of new neutrino telescopes. The IceCube collaboration plans to increase the volume of the detector to 5–10 km^3 with increased distance between strings with PMTs. As a result, the energy threshold will increase. The increase in the area of the surface veto-detector to 100 km^2 is also planned to suppress atmospheric showers from neutrinos and muons, which significantly increases the effective volume of the detector.

The KM3NET detector, with a searched volume of 3–6 km^3 and 12,000 PMTs, will be deployed in the Mediterranean Sea. The deployment is planned in three phases:

(1) proof of prototype's performance;

(2) measurement of astrophysical neutrino fluxes at the IceCube level;

(3) neutrino astrophysics research.

The Baikal-GVD experiment, with a sensitive volume of 1 km^3, is under deployment in Lake Baikal (see Section 3).

Neutrino telescopes have a diverse physical program: they will be used not only to study astrophysical neutrinos, their spectra, and their sources, but also to measure the neutrino mass hierarchy, to search for dark matter, for the neutrino tomography of Earth, and for other advanced studies.

2.7 Neutrino geophysics

Geoneutrinos are the antineutrinos from decays of natural radioactive β-decaying isotopes in Earth. The main contribution to the natural radioactivity of Earth is made by elements from decay chains of long-lived isotopes ^{238}U and ^{232}Th, as well as from ^{40}K decays.

Although the density profile in Earth is reconstructed from seismic data, the chemical composition of Earth's interior remains unexplored; therefore, the precise measurement of geoneutrino fluxes can be used to reconstruct the spatial distribution of neutrino-generating radioactive isotopes and thus offers the opportunity to determine the abundance of the corresponding radioactive elements.

Earth's natural radioactivity is a powerful source of heat affecting the thermal history of Earth, and the internal distribution of radioactive elements inside Earth needs to be known to solve many geophysical problems. The heat generation mechanism in Earth's interior is a fundamental geological problem. Measurements have shown that the thermal power of our planet is (47 ± 2) TW [130]. Radiogenic heat and the primordial heat stored by Earth during gravitational differentiation of matter are the main internal heat sources. Other sources contribute less than 1% to the total power.

Geoneutrino fluxes began to be investigated recently in parallel with the development of large-volume scintillation detectors with a high sensitivity to measure antineutrino fluxes at a level of $\sim 10^6$ cm^{-2} s^{-1} with an energy of a few MeV.

Measurements of the geoneutrino fluxes can shed light upon still open questions about the radioactivity of our planet: What is the radiogenic contribution to the total heat power of Earth? How much uranium and thorium is contained in Earth's crust and mantle? Is there a georeactor or a hidden ^{40}K source in the center of Earth, as suggested by

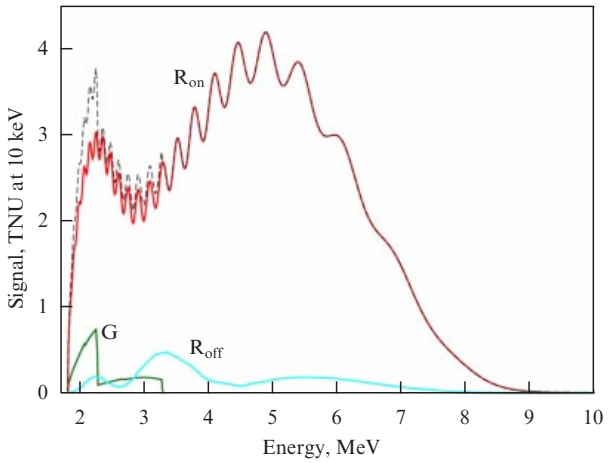

Figure 12. Expected geoneutrino signal in the JUNO detector (the G curve) compared to signals before turn-on (curve R_{off}) and after turn-on (curve R_{on}) of reactors in Yangjiang (17.4 GW) and Taishan (18.4 GW). The dashed curve corresponds to the total signal after turn-on of the detector. (From Ref. [134].)

some authors? Is the standard geochemical model of Earth consistent with geoneutrino data?

Experimental neutrino geophysics emerged as a science in 2005 after the first related publication by the KamLAND collaboration. The existence of geoneutrinos and, hence, the contribution of radioactive isotopes to Earth's heat power has been confirmed at the 4.2σ and 5.9σ levels in two independent experiments, KamLAND [131] and Borexino [132], respectively. The accuracy of measurements of the total geoneutrino fluxes in the analysis with a fixed U/Th mass ratio is so far low in both experiments, of the order of 30%. The analysis with a free U/Th mass ratio has not yielded reasonable constraints.

Presently, different geophysical models are in good agreement with measurements; however, to fix model parameters, more accurate measurements of the geoneutrino fluxes are required. On the other hand, it is already possible now to assert that exotic scenarios of Earth's heating due to an internal georeactor are ruled out, the contribution from such a reactor to the total heat power being less than 4.5 TW at the 95% CL according to the Borexino data [133] and below 3.7 TW according to the KamLAND experiment [131].

Third-generation reactor detectors (JUNO and RENO-50) will be sensitive to geoneutrinos. The JUNO detector sensitivity was recently estimated in [134] (Fig. 12). The expected geoneutrino signal[8] is $39.7^{+6.5}_{-5.2}$ TNU. The signal from reactors (in the 'geoneutrino' energy 'window'), as of 2013, is $26.0^{+2.2}_{-2.3}$ TNU. Thus, the measurement accuracy of the geoneutrino signal in this case is 10% for the data-taking duration of about 100 days.

After turning on nearby reactors in Yangjiang and Taishan, the reactor signal will increase to 354^{+45}_{-41} TNU, which will complicate detection of the geoneutrino signal. Nevertheless, the JUNO project [72] optimistically estimates the possibility of measuring the geoneutrino flux, despite the high reactor background. By assuming an 80% efficiency of the neutrino detection in an 18.35 kt volume of LS and fixed chondritic level of the U-to-Th mass ratio in Earth ($M(\mathrm{Th})/M(\mathrm{U}) = 3.9$), the statistical accuracy of the geoneutrino signal reconstruction is 17%, 10%, 8%, and 6% for 1, 3, 5, and 10 years of data taking, respectively.

Next-generation neutrino telescopes should offer interesting possibilities for determining the chemical composition of Earth's core. The idea of measuring Earth's composition is based on the dependence of neutrino oscillations on the electron density n_e in matter (neutrino tomography). Resonance oscillations of atmospheric neutrinos inside Earth, which are possible because of the relatively large value of the angle θ_{13}, can serve as a sensitive tool to determine the chemical composition of Earth's core.

The neutrino tomography of Earth will be one of the tasks of the upcoming PUNGU project. The extensive existing statistics on atmospheric neutrinos will be used to verify different models of Earth's core [76]. Systematic uncertainties related to oscillation parameters will be reduced due to detection of neutrino fluxes not passing through the core.

3. JINR neutrino program

Systematic experimental research in neutrino physics, weak interactions, rare processes, and astrophysics has been carried out at JINR in the Dzhelepov Laboratory of Nuclear Problems (LNP).

This almost 55-year-long tradition stemmed from the work and ideas of Pontecorvo and his colleagues. Researchers at LNP have obtained many fundamental results in this field.

First of all, the pion beta decay $\pi^+ \to \pi^0 e^+ \nu_e$ was discovered [135], which was direct proof of the vector current conservation in weak interactions, which was first theoretically predicted by Ya B Zeldovich and S S Gershtein.

Pontecorvo (together with Markov) justified the possibility of the existence of the muon neutrino and in 1959 proposed an experiment to detect this neutrino in high-energy accelerators [136], which was later performed in the USA, where muon neutrinos were actually detected. Pontecorvo and collaborators were the first who observed the recoil from the muon neutrino during the capture of negatively charged muons in helium-3, $\mu^- + {}^3\mathrm{He} \to {}^3\mathrm{H} + \nu_\mu$, which enabled imposing an upper bound on the mass of this particle. The experiment confirmed the identity of the muon and the electron in weak interactions ($\mu-e$ universality) [137]. The correctness of the vector–axial ($V-A$) structure of fermionic currents participating in weak interactions with charged $W^\pm$ bosons and the universality of weak interaction were confirmed by measurements of the probability of muon captures by protons, $\mu^- + p \to n + \nu_\mu$ [138].

Vylov and collaborators measured the helicity of electron neutrino in ^{152m}Eu decays using the Ge(Li) detector [139].

As mentioned in Section 1, in 1957, Pontecorvo put forward the idea of the possible existence of neutrino oscillations, the conversion of one neutrino flavor to another, which is possible in principle only if the neutrino has a nonzero mass [140, 141].

Pontecorvo initiated the first experimental work on the determination of the probability of decays forbidden by the lepton number conservation. At the LNP, using the ARES (Analyzer of Rare Events) device, a record bound on the $\mu \to 3e$ decay probability was obtained [142].

[8] The signal is measured in TNU (Terrestrial Neutrino Unit). 1 TNU corresponds to one interaction for every 10^{32} target protons per year. One kiloton of liquid scintillator contains about 10^{32} protons, and the exposure time in the corresponding experiments usually lasts several years. Thus, TNU counts the rate of inverse beta decays on a proton for a one-kiloton detector per year.

In 1957, Pontecorvo suggested the possible existence of transitions of muonium (an atom consisting of two leptons, $M \equiv \mu^+e^-$) into antimuonium $\overline{M}$ (μ^-e^+) [140]. In this process, lepton numbers of particles change not by one but by two, and the transition $\mu^+e^- \to \mu^-e^+$ is forbidden in the SM. In 1993, using the LNP phasotron, the upper bound on the $M \to \overline{M}$ transition was set [143, 144].

The development of neutrino physics and particle physics before 1983 can be traced using reviews by Pontecorvo and his colleagues [145–152], which demonstrated a remarkable simplicity and clarity of many complicated issues, as well as the special role played by JINR in this field.

The first accelerator neutrino experiments, in which JINR physicists played an important role, were carried out with the Neutrino Detector at the High Energy Physics Institute (Protvino) and NOMAD (Neutrino Oscillation MAgnetic Detector) at CERN, which performed a number of important measurements [153–167].

Presently, studies are carried out in the framework of the neutrino program that has been significantly extended and includes experimental and theoretical research in topical fields of neutrino physics.

All projects of the JINR neutrino program are thoroughly justified and have passed through internal and international expertise. The JINR neutrino program is expected to yield advanced results in neutrino physics. The development of experimental devices both in Russia and abroad is a necessary condition for the successful realization of the neutrino program. Here are the three most important avenues.

First is the development of the Baikal-GVD experiment. A 1 km^3 neutrino telescope is under construction on Lake Baikal. In 2015, the first cluster of the telescope, called Dubna, was deployed. This experiment is extremely important in connection with the first detection of astrophysical ultra-high-energy neutrinos in the IceCube experiment, which opens up a new area in physical studies — 'neutrino ultra-high-energy astrophysics'. The upgraded Baikal-GVD installation should play an important role in these studies.

Second, a neutrino laboratory successfully operates at the Kalinin NPP. Here, JINR is the principal investigator of the unique experiments GEMMA (measurements of the magnetic moment of antineutrinos), DANSS (search for sterile neutrinos and monitoring of antineutrinos from Kalinin NPP), and νGeN (ν–Ge Nucleus elastic scattering) (measurement of the neutrino-nucleon coherent scattering cross-section).

Third, JINR considers it necessary to participate in the most ambitious and important international projects in neutrino physics, making significant intellectual and financial contributions into them. Presently, these projects include:

— experiments in the low-background underground laboratories Gran Sasso (Borexino, Dark Side, GERDA) and Modan [EDELWEISS (from French Expérience pour Detecter les wimps en site Souterrain) and SuperNEMO (Super Neutrino Majorana Observatory)];

— experiments with reactor antineutrinos (Daya Bay, JUNO);

— experiments with accelerator neutrinos (antineutrinos) (NOνA).

A detailed description of the JINR neutrino program can be found in the JINR White Book [168]. Below, we briefly describe the most important results of the neutrino experiments obtained with the active participation of JINR researchers and discuss the expected results and prospects of new projects.

OPERA (*Oscillation Project Emulsion-tRacking Apparatus*) *experiment* is a long baseline neutrino experiment aimed at discovering tau neutrinos in a muon neutrino beam. The distance between the neutrino source at CERN and the OPERA detector in Gran Sasso is 730 km. A hybrid detector consisting of two targets was used. Each target was equipped with a muon spectrometer. The target of the OPERA detector consisted of walls filled with 'emulsion bricks', and plastic scintillator detector planes served for targeting purposes. The emulsion bricks consisted of 56 lead layers 1 mm in thickness each, alternating with photoemulsion films providing micrometer accuracy in measuring tracks of charged particles. The OPERA detector contained about 150,000 such bricks. The total mass of the detector was around 1.2 kt.

The neutrino beam was directed from CERN to Gran Sasso (CNGS — Cern Neutrino to Gran Sasso) for five years from 2008 to 2012. In total, the target at CERN was bombarded by 17.97×10^{19} protons, which enabled the detection of 19,505 neutrino interactions in the detector. To date, five ν_τ candidates have been observed. The expected numbers of the true and background events are respectively 2.64 ± 0.53 and 0.25. The OPERA collaboration reported the discovery of ν_τ in the CNGS beam at the confidence level of five standard deviations (5σ) [169].

Presently, the OPERA collaboration is completing the data analysis, and the OPERA detector is being dismantled. Part of this detector (targeting detector) will be used in the JUNO experiment.

The *Daya Bay experiment* measured the before-unknown angle θ_{13}, the result was one of the most significant ones of the most significant results in particle physics in 2012. Later, in 2013, the effective difference in the mass squares Δm^2_{ee} was measured. In 2015, the Daya Bay experiment obtained the results [170]

$$\begin{aligned} &\sin^2(2\theta_{13}) = 0.084 \pm 0.005\,, \\ &|\Delta m^2_{ee}| = (2.42 \pm 0.11) \times 10^{-3}\ \text{eV}^2\,. \end{aligned} \tag{20}$$

By 2017, the precision of measurements of $\sin^2(2\theta_{13})$ in the continuing Daya Bay experiment is expected to be around 0.00307. The joint analysis of data obtained by the Daya Bay, Double Chooz, and RENO experiments will allow measurement of $\sin^2(2\theta_{13})$ in the confidence interval ± 0.00282 [171]. The value of Δm^2_{ee} will be determined within the confidence interval $\pm 7 \times 10^{-5}\ \text{eV}^2$, i.e., to a 3% accuracy [171]. Figure 13 illustrates how these estimates will change with time.

The location of the Daya Bay detectors relative to the Daya Bay, Ling Ao, Ling Ao II reactors corresponds to nine different detector–reactor distances. This enabled physicists to set new upper bounds on the mixing parameters of the hypothetical sterile neutrino $\sin^2(2\theta_{14})$, $|\Delta m^2_{41}|$ in the previously unexplored range $10^{-3}\ \text{eV}^2 \leqslant |\Delta m^2_{41}| \leqslant 0.1\ \text{eV}^2$ [172].

In 2012, the Daya Bay collaboration measured the flux of reactor antineutrinos [173]. The measured flux, which is in agreement with previous data from short-distance experiments, is 0.946 ± 0.02 from the model flux in [174, 175] and 0.991 ± 0.023 from the model flux in [176–179]. The measured form of the positron spectrum differs by 2σ from the predictions in [174, 175] in all energy ranges by reaching the local significance 4σ in the energy range 4–6 MeV. This result is confirmed by the data of the RENO and Double Chooz experiments.

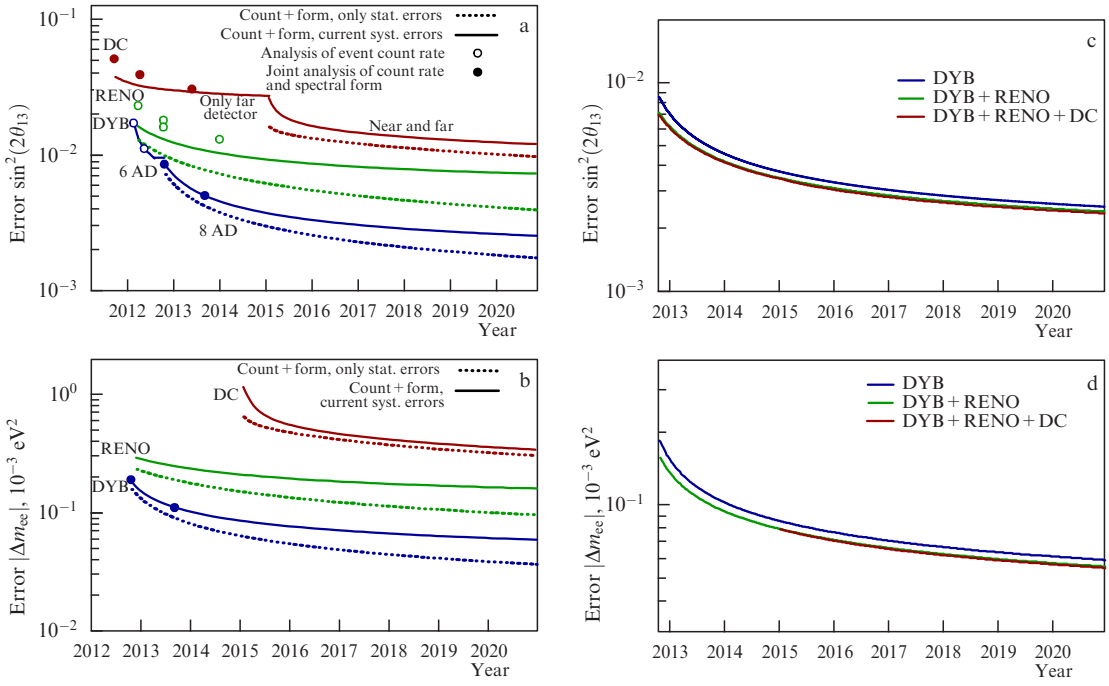

Figure 13. Expected experimental errors of (a) $\sin^2(2\theta_{13})$ and (b) $|\Delta m^2_{ee}|$ as a function of time for each of the experiments Double Chooz (DC), RENO, and Daya Bay (DYB) (AD is the antineutrino detector). The expected measurement errors of (c) $\sin^2(2\theta_{13})$ and (d) $|\Delta m^2_{ee}|$ as a function of time from joint analysis of these experiments [171].

The members of the Daya Bay collaboration jointly with KamLAND, K2K/T2K, Super-Kamiokande, and SNO were awarded the biggest world scientific prize — the 2016 Breakthrough Prize in Fundamental Physics.

The Borexino experiment. The international Borexino collaboration has been taking data from a 300 ton LS detector since 2007. Physicists from JINR have been participating in the experiment since 1991. The Borexino detector was designed for real-time studies of low-energy solar neutrinos, first and foremost monoenergetic ones (with the energy 862 keV) from the reaction $^7\mathrm{Be} + \mathrm{e}^- \to {}^7\mathrm{Li} + \nu_\mathrm{e}$.

To detect neutrinos with such energies, an extremely pure detecting medium is required, because decays of natural radioactive impurities, which are present to some extent in any natural materials, can mimic neutrino interactions.

Therefore, significant efforts in the Borexino project have been aimed at selecting radioactively pure materials for the detector and developing new techniques of purification of liquids and gases from natural radioactive admixtures. As a result of studies that lasted for more than 10 years, a record high level of purification of a liquid organic scintillator was reached in Borexino. For example, the amount of U/Th admixtures in the liquid scintillator is $\approx 10^{-17}$ g/g; the amount of ^{40}K is $\leqslant 10^{-14}$ g/g; the amount of ^{14}C is $\sim 2.7 \times 10^{-18}$ g/g (relative to ^{12}C). Due to the high purification level, the high-sensitivity detector constructed by the Borexino collaboration turned out to be suitable for detection of neutrinos from other solar reactions and is sensitive to geologic and reactor antineutrinos. The results obtained by the Borexino experiment, in particular, include the direct measurement of the solar neutrino flux from the pp reaction [109] and the first statistically significant observation of geoneutrinos [180].

The Borexino experiment measured the solar beryllium neutrino flux with a 5% accuracy [111], as well as its daily [181] and seasonal [182] variations. In addition to beryllium neutrinos, fluxes of boron neutrinos [183] (this measurement, of course, has a lower accuracy than measurements with large water Cherenkov neutrino detectors, but is the first measurement of the high-energy part of the solar neutrino spectrum by an LS detector), pep neutrinos [110], and pp neutrinos [109] were measured. Thus, neutrino fluxes from all the main reactions of the pp chain were measured for the first time by one detector. Borexino also measured the geoneurino flux from decays of natural radioactive isotopes in Earth [184]; today, this measurement, together with the KamLAND detection, provides unique information on the uranium and thorium content in Earth's interior.

In addition to neutrino flux measurements, the Borexino experiment has searched for rare events beyond the SM according to the program proposed by scientists from Dubna. Presently, the experiment is establishing the best upper bounds on the effective magnetic moment of solar neutrinos [185], on the axion flux from the Sun [186], and on the Pauli principle violation [187]. Constraints on the lifetime of the electron with respect to the decay $\mathrm{e} \to \nu + \gamma$ ($T_{1/2} \geqslant 6.6 \times 10^{28}$ years) [188] were improved by more than two orders of magnitude.

The main results were obtained by the collaboration using data collected prior to 2010, during the first stage of the experiment. In 2010, after the detector calibration, additional purification of the scintillator was performed. Due to good stratification (the scintillator layers do not mix in the process of filling out and filling up), a few purification cycles enable removing ^{85}Kr from the scintillator, which is the main source of systematic error in spectral fitting. The ^{210}Bi counting rate here was reduced to 20 events per day for every 100 t of the scintillator. Presently, during the second stage of the experiment, the statistics have been taken over an almost four-year running time with the 'pure' scintillator, and data taking

continues. An analysis of the pp-neutrino flux has been carried out using the data collected in the first two years of the second phase.

Measurement of the CNO-cycle solar neutrinos has been the main goal of the second phase of the Borexino experiment. The interest in the CNO neutrinos has increased due to the solar metallicity problem discussed in Section 2.5. Measuring CNO neutrinos even with modest accuracy would allow distinguishing between different models, because the predicted CNO neutrino fluxes are very different for low and high solar metallicity. The Borexino experiment obtained an upper bound on the CNO-neutrino flux: assuming the model with neutrino oscillations, the CNO-neutrino flux is $< 7.4 \times 10^8$ cm^{-2} s^{-1} (90% CL), which is in agreement with predictions of both variants of the standard solar model. This result demonstrates the fundamental possibility of a more precise measurement of pep and CNO neutrinos if the systematic uncertainty due to the correlated background from radioactive ^{210}Bi decays is further reduced.

The SOX project. The Borexino experiment planned measurements with a neutrino source to calibrate the detector, and the antineutrino source ^{90}Sr–^{90}Y was originally proposed. Later, it was proposed to also use the source of monoenergetic neutrinos based on ^{51}Cr [189]. This source was successfully employed to calibrate the GALLEX experiment. In connection with searches for sterile neutrinos actively discussed in recent years, the idea of measurements with additional neutrino sources is becoming more attractive: due to the large geometric size of the Borexino detector, it is possible to search for oscillations inside it with the characteristic length of about 1 m, which corresponds to $\Delta m^2 \sim 1$ eV^2.

The SOX project [100] plans to carry out measurements using an external ^{51}Cr neutrino source (located 8.25 m from the detector center) with the activity 5–10 MCi (phase A, or CrSOX) and with the antineutrino source ^{144}Ce (CeSOX) with the activity 50–150 kCi, installed in a water buffer at a distance of 7.15 m from the detector center (phase B) or in the detector center (phase C). The sensitivity of three phases of the experiment to oscillation parameters is presented in Fig. 14. Calculations were done for the ^{51}Cr source with the activity 10 MCi and for the ^{144}Ce source with the activity 75 kCi. Due to the complexity of activation of a Cr-based source, the experiment with the antineutrino source based on ^{144}Ce installed in a water buffer will be carried out first. Measurements will start after the source is delivered to the Gran Sasso laboratory at the end of 2016. Calorimeters to precisely measure the source activity (at the 1% level) are under construction.

Baikal-GVD experiment. Pioneering neutrino research in Lake Baikal began more than 35 years ago. Since then, extensive experience was accumulated and important results were obtained. The technology of neutrino detection by large deep-underwater detectors was developed. In 2006–2010, all key elements and units of the GVD detector were designed, manufactured, and tested.

A new phase of the experiment began in 2014. The discovery of astrophysical neutrinos by the IceCube detector opened new prospects for neutrino telescopes, because it became clear that telescopes with good angular resolution are required to identify high-energy neutrino sources. The Baikal collaboration optimized the installation and formulated new requirements on the parameters of the new detector [191].

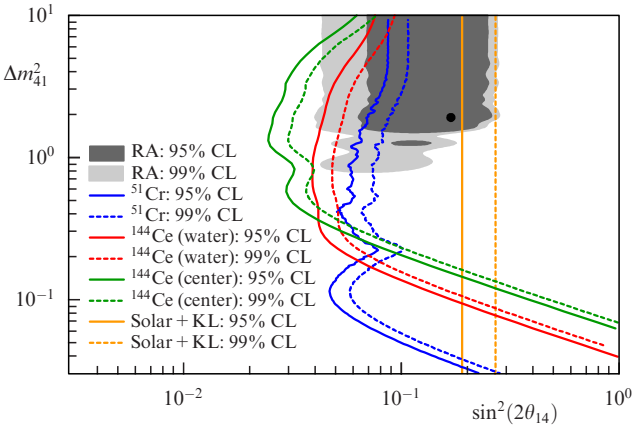

Figure 14. (Color online.) SOX experiment sensitivity to oscillation into sterile neutrinos in the phase A (external source ^{51}Cr, blue curve), phase B (source ^{144}Ce–^{144}Pr, red curve) and phase C (source ^{144}Ce–^{144}Pr in the center of the detector, green curve); Solar + KL show solar experiments + KamLAND. The gray area corresponds to the reactor anomaly (RA) interpreted in terms of oscillations into sterile neutrinos, the filled black circle in this area corresponds to the RA best fit. In all cases, 90% and 95% CL contours are shown. The yellow curve bounds the region excluded by other experiments [190].

The basic element of the experiment is the optical module (OM) consisting of a 10-inch PMT Hamamatsu-R7081HQE with high quantum efficiency (up to 35%), a high-voltage PMT power supply setup, a controller, a protection system of the PMT from the terrestrial magnetic field, and a calibration system with a photocathode. All elements of the OM are placed into a sealed deep-underwater spherical glass container (Fig. 15).

The optical modules are attached to vertical cables forming strings. The main structure unit of a string is the OM section. A section is a functionally completed detector unit, including blocks of emission registration, signal processing, and data transferring. The structure of the data taking system in each section enables forming different configurations of optical modules. Individual or pairs of OMs can be placed at different spacings. Several sections can be mounted on each string in different configurations. The configuration of a section, which is presently the base for further design, includes 12 optical modules with a 15 m spacing along the string, a central module (CM) of the section located in the middle of the section, and a service module (SM). Analog signals from the OM of a section are transmitted to the CM by identical 100 m coaxial cables. These cables are also used for low-voltage power supply of the OM.

In the CM, the analog signals from optical modules are digitized and transmit the information via an Ethernet line. The service module is used for time calibration, determination of the string location, and the power supply of the OM. Electric power supply synchronization and data transmission from sections are combined in the commutation module of the string, which is connected by 1200 m cables with the central control block of the cluster. The data are transmitted using Ethernet technology. The basic cluster configuration includes eight strings, each with 24 OMs (two sections on a string), separated by 60 m from each other.

The clusters of the strings are connected to a data processing center on the shore by 6 km combined fiber-optic cables. Each cluster of the telescope represents a functionally

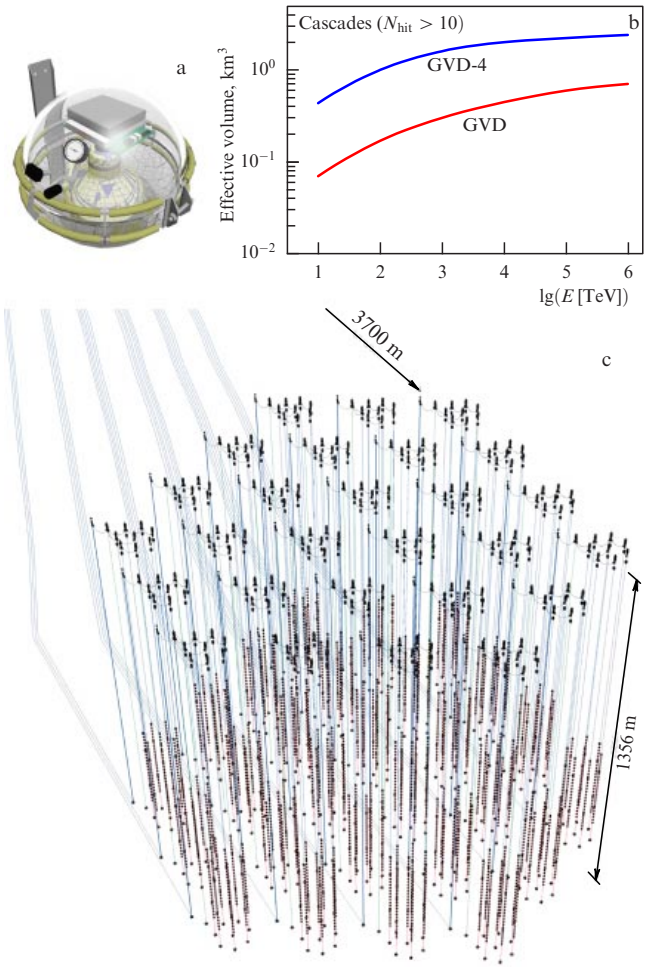

Figure 15. (a) Optical module of the Baikal-GVD detector. (b) The effective volume of detection of neutrino-induced cascades as a function of their energy. Baikal-GVD includes 2304 OM, Baikal-GVD-4 includes 10,368 OM. (c) 27 clusters of the Baikal-GVD-4 detector.

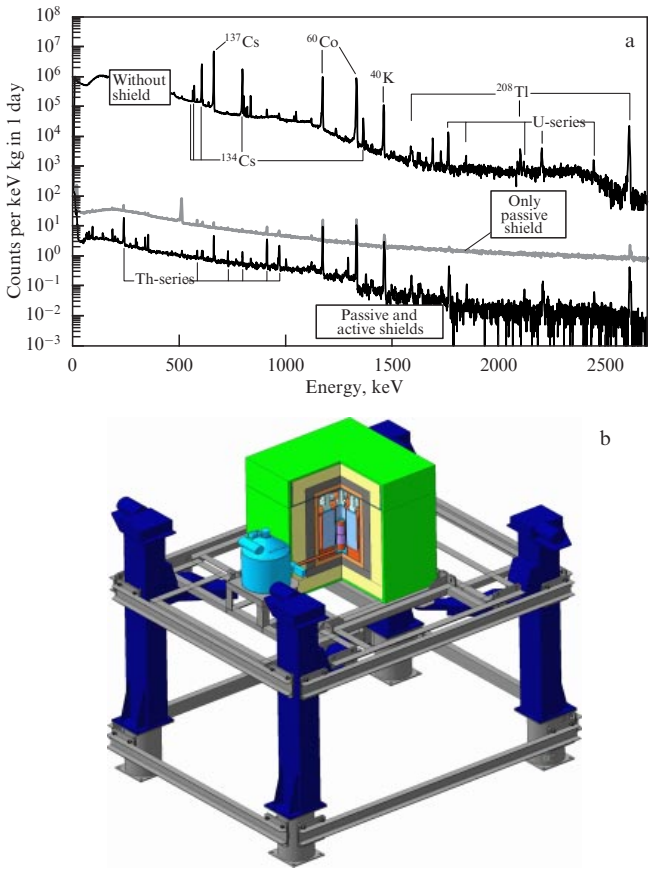

Figure 16. (a) Gamma spectrum measured under the reactor of the Kalinin NPP in different conditions (without a shield, with a passive shield, and with passive and active shields). (b) The GEMMA-II spectrometer on the mobile mechanism.

completed detector, which can operate either as part of the whole system or autonomously. This provides simplicity in building up the installation and the possibility of putting the individual units in operation during the development of the neutrino telescope. The cluster sensitive volume will be comparable to the ANTARES volume. It is expected that the cluster will register one astrophysical neutrino with the energy above 100 TeV a year.

The first phase of the construction of the Baikal-GVD experiment should be completed in 2020 with the installation of 12 clusters with 2304 OMs spaced 300 m apart. The instrumental volume of the detector will be 0.4 km^3. The physically observed volume depends on the neutrino energy and increases with energy, as shown in Fig. 15b. By the time of completion, the detector should be able to register 27 events from interactions of astrophysical neutrinos with energies above 100 TeV.

The expected accuracy of the event direction reconstruction is $3.5^\circ - 5.5^\circ$ for cascade-generating neutrino interactions and 0.25° for muon tracks.

The Baikal-GVD collaboration plans to further increase the detector volume to an instrumental value of 1.5 km^3. This installation will include 27 clusters of four sections each. The total number of OMs will be 10,368. The general view of the experiment is shown in Fig. 15a.

The main goal of the *GEMMA-II experiment* is to measure or further constrain the value of the neutrino magnetic moment (see Section 1.6). The new GEMMA-II detector will have better sensitivity to the neutrino magnetic moment than the previous detector GEMMA (Germanium Experiment for measurement of Magnetic Moment of Antineutrino). The new device includes two 3 kg germanium detectors with an effective detection threshold decreased from 2.8 keV to 1.5 keV.

The detector is placed inside a NaI crystal with a wall thickness of 14 cm, surrounded by a 5 cm layer of electrolytic copper and a 15 cm layer of lead. The detector, mounted on a mobile platform at a distance of 10 m under the nuclear reactor, is well protected from the hadron component of cosmic rays by the reactor itself and the technological equipment. The muon flux is reduced by 10 times within the solid angle $\pm 20^\circ$ near the vertical and 10-fold within the solid angle $\pm(70^\circ - 80^\circ)$. Surrounding the detector mentioned above is passive shielding. The remaining muons, by interacting with the detector's protection, produce fast neutrons that interact elastically in the germanium detector and increase the low-energy background. To suppress this background, the detector is surrounded by an additional shield made of a plastic scintillator with an electronic readout, which enables detection of atmospheric muons. This additional protection is active. The result of using both passive and active protections is shown in Fig. 16a.

Additional control of the signal-to-background ratio in the experiment is performed by the mobile platform on which the detector is mounted (Fig. 16b). The distance between the detector and reactor centers can vary from 10 to 12 m.

Special measures are taken to protect the device from noise caused by mechanical vibrations, electric power interference, leakage of radioactive argon and xenon from the cryostat, and the intrinsic noise of germanium detectors. As a result, systematic uncertainties of measurements were significantly reduced and the detector sensitivity to the neutrino magnetic moment was increased to $1 \times 10^{-11}\mu_B$.

In the future, it is planned to use a new detector with point contacts, which enables the effective detector threshold to be reduced to 300 eV. The use of several detectors with a total mass of 5 kg will allow increasing the sensitivity to the neutrino magnetic moment to $(5-10) \times 10^{-12}\mu_B$ [168].

The JUNO experiment will try to measure the neutrino mass hierarchy using an underground LS detector located at a distance of 53 km from the Yangjiang and Taishan nuclear power plants in Guangdong province (China). The experimental hall with a length of more than 50 m located under a mountain is protected from cosmic radiation by a 700 m granite layer. During six years of operation of the detector, the neutrino mass hierarchy can be measured at the confidence level of $(3-4)\sigma$. To fulfill this task, the antineutrino energy should be reconstructed with a resolution better than 3% for a released energy of 1 MeV with an absolute accuracy of the energy scale better than 1%. In view of the large mass of the detector, when this accuracy in energy reconstruction is attained, it will be possible to measure the parameters $\sin^2\theta_{12}$, Δm^2_{21}, and $|\Delta m^2_{ee}|$ with an accuracy better than 1%.

The multi-purpose JUNO detector can observe neutrinos (antineutrinos) from terrestrial and extraterrestrial sources, including neutrinos from supernovae, diffuse neutrinos from supernovae, geoneutrinos, atmospheric neutrinos, and solar neutrinos, which enables investigating many questions of neutrino physics and astrophysics. JUNO is also sensitive to physics beyond the SM, including sterile neutrinos, neutrinos from dark matter annihilation, and proton decays, as well as nonstandard neutrino interactions and Lorentz-violating and CPT-violating processes.

The central detector of JUNO contains 20 kt of liquid scintillator surrounded by 17,000 PMTs. The expected stable operation time of the detector is more than 20 years. The liquid scintillator will be placed into an acryl sphere 35 m in diameter supported by a stainless steel construction. The requirements to the LS include a light yield and transparency, as well as low radioactive contamination level.

A muon veto system will be used to suppress atmospheric muon backgrounds. The muon veto includes a water Cherenkov detector and an upper tracker. The target detector from the OPERA experiment that completed operation will be used as the upper tracker. The water Cherenkov detector consists of a pool filled with purified water and PMTs mounted on the pool walls. The central detector with a liquid scintillator will be placed at the center of the water pool.

PMTs registering scintillation photons from the central detector will be mounted on a spherical surface about 38 m in diameter. To reach the required resolution, they must provide 75% of the total geometric coverage of the sphere. Here, about 17,000 PMTs with a diameter of 508 mm (20 inches) are required. Additionally, about 1600 PMTs are directed away from the central detector in order to register Cherenkov photons. The possibility is also being considered of using three-inch PMTs in the free space between large 20-inch PMTs, two small ones per large one. The use of small PMTs with better time characteristics will enable significant improvement in reconstructing the interaction point inside the detector and hence in the sensitivity.

To reduce the effect of the terrestrial magnetic field on the PMT performance, a system of coils with currents placed around the central detector inside the water pool will be used.

The determination of the neutrino mass hierarchy in the experiment is impossible without a careful calibration of the algorithm of the event vertex and energy reconstruction. The calibrations can be done using different sources (light, γ, e^+, e^-, n, and α) imitating interactions inside the detector in the entire energy range of the inverse β-decay. The calibration system should allow placing the source at any point of the central detector. An ultrasonic positioning system will enable the source coordinate determination with an uncertainty of less than 3 cm. Several additional calibration subsystems are considered that can overlap different parts of the central detector with different periodicity of their use.

The JUNO electronics include two blocks for the central detector and a veto detector. Their main goals are to read the PMT signal from two subdetectors and to process and transfer data to the data collection system. To avoid data loss during long-distance data transfer, most of the electronics will be located in the water pool near the detectors. The expected data flux is 2 Gb s^{-1}. In the case of a supernova explosion at a distance of 10 kpc from Earth, the data flux increases to 10 Gb s^{-1}. The experimental data from JUNO will be processed with a dedicated computer farm including 10,000 cores with a disk memory of 10 Pbyte (10^{16} bytes).

Figure 17 illustrates the principle of the mass hierarchy determination used in the JUNO experiment, as well as the main challenge to the experiment — the energy reconstruction level not worse than 3% for 1 MeV of the energy released. The detector is planned to be mounted and filled with a liquid scintillator in 2019, and full-scale data taking will begin in 2020.

The NOvA experiment is a multi-purpose experiment. The main goal is to measure the neutrino mass hierarchy and the phase δ responsible for CP-violation in the lepton sector. The NOvA experiment uses two detectors, the near and the far ones. The near detector is placed at a depth of 100 m at the Fermi National Accelerator Laboratory (Fermilab) (USA) about 1 km away from the target part of the NuMI beam. The mass of the near detector is 0.3 kt. The far detector with a mass of 14 kt is placed at a distance of 810 km from the neutrino source. The basic element of both detectors is a polyvinylchloride cell $1560 \times 4 \times 6$ cm in size filled with a liquid scintillator. An optical fiber is used inside the cell as the output for the scintillation light produced by charged particles passing through the scintillator. The scintillation light is registered by a 32-channel avalanche photodiode. The cells form the detector layers, whose vertical and horizontal orientations can be used to measure the x and y coordinates of particle tracks. The positions of the near and far detectors are shown in Fig. 18a. Both NOvA detectors are shifted from the beam axis by the angle of 14 mrad, at which the beam spectrum with a peak energy at 2 GeV is more narrow than that of the on-axis beam.

The neutrino mass hierarchy in this experiment manifests itself as different probabilities of oscillations $P(\nu_\mu \to \nu_e)$ and $P(\bar{\nu}_\mu \to \bar{\nu}_e)$, as shown in Fig. 18b. The oscillation probabilities

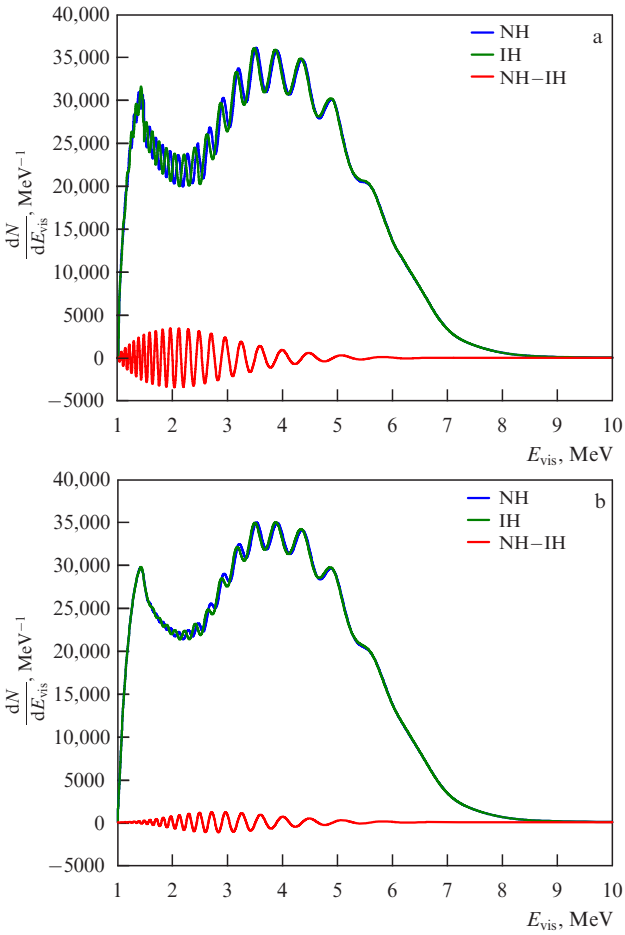

Figure 17. (Color online.) Expected spectrum of visible energy in the JUNO experiment for $|\Delta m^2_{ee}| = 2.44 \times 10^{-3}$ eV^2 (a) assuming ideal energy resolution and (b) $\sigma_E = 3\%$ [168].

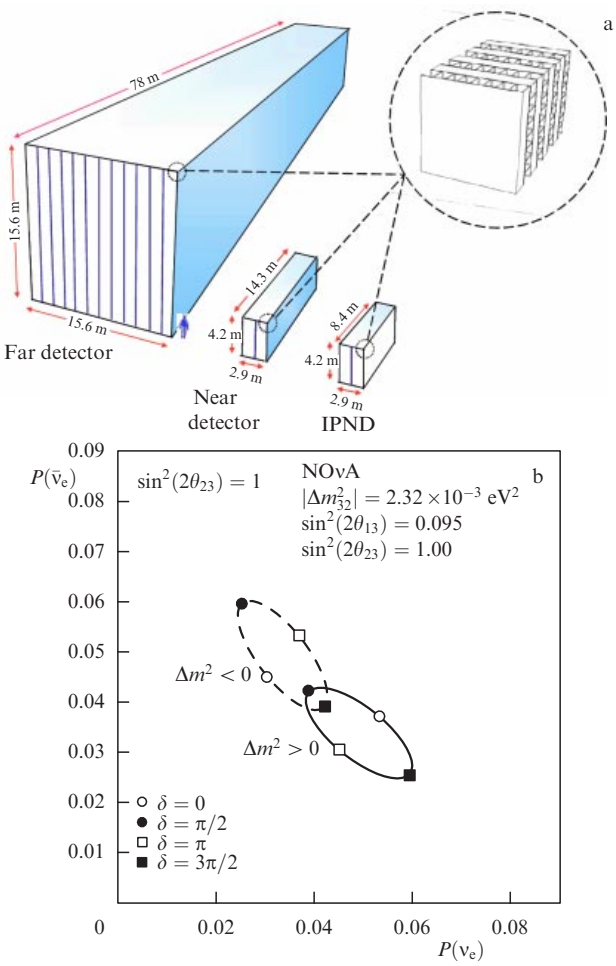

Figure 18. (a) Far and near NOνA detectors (IPND — Integrated Prototype Near Detector). The basic element of the detector includes a plastic cell with a liquid scintillator inside and light-conducting optical fiber. (b) Probabilities of oscillations $P(\nu_\mu \to \nu_e)$ and $P(\bar{\nu}_\mu \to \bar{\nu}_e)$ for the fixed ratio $L/E = 0.4$ km MeV^{-1} and four values of the phase δ [192].

depend, however, not only on the neutrino mass hierarchy but also on the phase δ and values of $\sin^2(2\theta_{13})$ and $\sin^2(2\theta_{23})$. Results of the experiment can be uncertain due to some parameter degeneracy. For example, if both probabilities turn out to be of the order of $P(\nu_\mu \to \nu_e) \simeq P(\bar{\nu}_\mu \to \bar{\nu}_e) \simeq 0.4$, the NOνA experiment will be unable to distinguish the normal hierarchy with $\delta = \pi/2$ from the inverted one with $\delta = 3\pi/2$. However, even in the worst case, NOνA will exclude some possibilities (the inverted hierarchy and $\delta = \pi/2$, the normal hierarchy and $\delta = 3\pi/2$). NOνA plans to accumulate data for six years: three years in the neutrino mode and three years in the antineutrino mode. The experiment started running in the neutrino mode in 2015, and the first results based on 7.6% of the total expected statistics were presented in the summer of 2015 [193].

First of all, the $\nu_\mu \to \nu_\mu$ mode was investigated. The spectrum measured in the near detector was used to reduce systematic errors due to uncertainties in the neutrino–nucleus interaction cross section. In the absence of oscillations, 201 events from ν_μ interactions were expected in the far detector. Only 33 events were detected. This number perfectly fits a neutrino oscillation model with

$$\Delta m^2_{32} = \begin{cases} +2.37^{+0.16}_{-0.15} \times 10^{-3}\ \text{eV}^2, & \text{normal hierarchy}, \\ -2.40^{+0.14}_{-0.17} \times 10^{-3}\ \text{eV}^2, & \text{inverted hierarchy}, \end{cases} \qquad (21)$$

$$\sin^2(2\theta_{23}) = 0.51 \pm 0.10\,.$$

The measurement accuracy attained using such small statistics is only slightly worse than that obtained in the MINOS (Main Injector Neutrino Oscillation Search) and T2K experiments, confirming a significant potential of the NOνA experiment.

The next mode explored in NOνA was $\nu_\mu \to \nu_e$. The ν_e identification was performed in two somewhat different ways. The first used the Likelihood IDentification (LID) function, while the second employed the identification of an event most similar to ν_e in the data (Library of Event Matching, LEM). Both methods have a similar efficiency and purity in selecting ν_e events.

Both methods predict about one background event in the far detector. The LID (LEM) method predicts 5.62 ± 0.72 (5.91 ± 0.65) signal events, assuming $\theta_{23} = \pi/4$ and the normal hierarchy with $\delta = 3\pi/2$, and 2.24 ± 0.29 (2.34 ± 0.26) events in the case of the inverted hierarchy with $\delta = \pi/2$. These estimates provide bounds on the measurement. The expected number of events for other values of the parameter δ falls within this range.

Six ν_e events were found in the data by the LID method and 11 events by the LEM method. Both methods confirm $\nu_\mu \to \nu_e$ oscillations at 3.3σ (LID) and 5.5σ (LEM) confidence levels. The normal hierarchy with δ around $3\pi/2$ is favored in

both methods. So far, the confidence level is not very high, $(1-2)\sigma$, but the statistical significance of the final results of the experiment is expected at the 3σ level.

The GERDA experiment. Until recently, the claim in [85] of the observation of double inverse beta decay has been neither refuted nor confirmed. Presently, the most sensitive experiments searching for double neutrinoless beta decay include experiments with the ^{136}Xe isotope and the GERDA experiment, which employs germanium detectors enriched to 86% with ^{76}Ge that were taken from HdM and IGEX (International Germanium EXperiment) experiments. Due to the different matrix elements for different isotopes, a comparison of results of the ^{136}Xe and ^{76}Ge experiments is model-dependent; therefore, only the GERDA experiment can directly confirm (or refute) the claim.

The GERDA experiment is being carried out in several stages. The first stage finished in 2013; its goal was to check the results in [85] with an exposition of 20 kg year.

The data obtained during the first phase of the GERDA experiment did not reveal a peak at the energy $Q_{\beta\beta}$, i.e., the claim about the observation of double neutrinoless beta decay of ^{76}Ge has not been confirmed. Assuming $T_{1/2}^{0\nu}$ from [85], the expected number of events is 5.9 ± 1.4 in the energy range $\pm 2\sigma_E$ (σ_E is the energy resolution of the detector) near $Q_{\beta\beta}$ with 2.0 ± 0.3 background counts after the pulse shape discrimination. These values should be compared to three events detected in this energy range, all of them falling outside the energy range $Q_{\beta\beta} \pm \sigma_E$. The H_1 hypothesis, which assumes the neutrinoless double beta decay, is in worse agreement than the H_0 hypothesis, assuming the presence of only the background: the probability ratio of both hypotheses is $P(H_1)/P(H_0) = 0.024$. According to the H_1 model, the probability of a null signal ($N^{0\nu} = 0$) is only $P(N^{0\nu} = 0|H_1) = 0.01$.

The result of the first phase of the GERDA experiment [89] is compatible with the HdM [194] and IGEX [195] bounds. The likelihood function profile was extended to include the energy spectrum of the HdM experiment (2000–2080 keV) (see Fig. 4 in [194]) and IGEX experiment (2020–2060 keV) (see Table II in [195]). The data processing assumed a homogeneously distributed background for each of five data sets and a Gaussian signal with the same lifetime $T_{1/2}^{0\nu}$. The experimental parameters (exposition, energy resolution, efficiency) available from the original publications or extrapolations from the GERDA detector data were used. The best fit corresponds to $N^{0\nu} = 0$ and the lifetime upper bound

$$T_{1/2}^{0\nu} > 3.0 \times 10^{25} \text{ years (90\% CL)}. \qquad (22)$$

The probability ratio is $P(H_1)/P(H_0) = 2 \times 10^{-4}$. Thus, the hypothesis of the observation of double neutrinoless beta decay has a very low probability.

At the next stage (GERDA Phase II), a sensitivity corresponding to $> 10^{26}$ years is expected after an exposure of 100 kg year with a background rate of $\lesssim 10^{-1}$ events per keV, the latter being more than an order of magnitude lower than at the first stage of the experiment.

To reach such a low background, the collaboration intends to employ about 30 additional detectors with a total mass of ≈ 20 kg of ^{76}Ge with a new geometry of electrodes (BEGe detectors[9] [196]), which improves the differentiation between beta and gamma signals. The new detectors will be placed in liquid argon, which enables detection of scintillation flashes from background radiation sources, thus providing an anti-Compton veto in the regime of coincidence with a signal from germanium detectors.

The *NEMO-3 experiment* in the Modane underground laboratory (Laboratoire Souterrain de Modane — LSM) has sought neutrinoless double beta decay. Measurements of several isotopes have been carried out since 2003: ^{48}Ca, ^{82}Se, ^{96}Zr, ^{100}Mo, ^{116}Cd, ^{130}Te, and ^{150}Nd. The principal targets were ^{100}Mo with a mass of about 7 kg and ^{82}Se with a mass of 1 kg. The lack of signatures of neutrinoless double beta decay resulted in a 90%-CL upper bound on the probability of this process, and an upper bound on the effective Majorana neutrino mass was obtained. In addition, NEMO-3 precisely measured the two-neutrino decay mode for several isotopes, which is permitted by the SM. Measurements of this process are important in order to decrease the uncertainty in nuclear matrix elements. The period of double beta decay of ^{130}Te was also accurately measured and compared to contradictory results of geochemical experiments.

Super-NEMO is a next-generation experiment employing the same track-calorimetry technique that was successfully used in NEMO-3. Due to the unique capability of tracking and identifying particles, Super-NEMO offers the possibility of both detecting neutrinoless double beta decay and determining its underlying mechanism. In Super-NEMO, as in NEMO-3, the source and detector are separated, and the experiment allows studying several isotopes, including ^{48}Ca, ^{82}Se, and ^{150}Nd. The total mass will be around 100–200 kg, enabling the sensitivity longer than 10^{26} years to half-life periods, which corresponds to a Majorana neutrino mass of about 50 meV, depending on the value of matrix elements. The prototype manufacturing was completed in 2015. The international collaboration on the project now faces the following pressing problems: producing sources in the form of thin foil with the required radiation purity, achieving good energy resolution of the calorimeter, and upgrading the construction of the track block of the detector. To control the required high level of radiation purity, several versions of the BiPo detector have been developed [199], one of which is already successfully running at the Canfranc underground laboratory (Spain).

The *DANSS project* plans to develop a relatively compact neutrino spectrometer based on a plastic scintillator, which can be placed near the active zone of a powerful industrial reactor (Fig. 19). In the sensitive 1 m^3 zone of the detector, nearly 10,000 inverse beta decay (IBD) reactions are expected a day if placed at the Kalinin NPP at a distance of 10 m from the reactor. The plastic scintillator segmentation allows a $\approx 1\%$ background suppression. Numerous tests carried out with a simplified prototype DANSSino at the Kalinin NPP under the reactor with a thermal power of 3 GW have demonstrated the performance capability of this concept. Background conditions at the Kalinin NPP have been studied. The general concept of the detector was probed and constructive improvements were implemented. The spectrum of the reactor antineutrinos was measured. Presently, the detector is under assembly.

Using a lifting mechanism, the DANSS detector will be able to move, together with a shield, over distances from 9.7 to 12.2 m from the active zone, enabling searches for sterile neutrinos with $\Delta m^2 \simeq 1$ eV^2. The sensitivity estimate (90% CL) of the DANSS experiment in one year of measurements is

[9] BEGe — Broad Energy Germanium detectors.

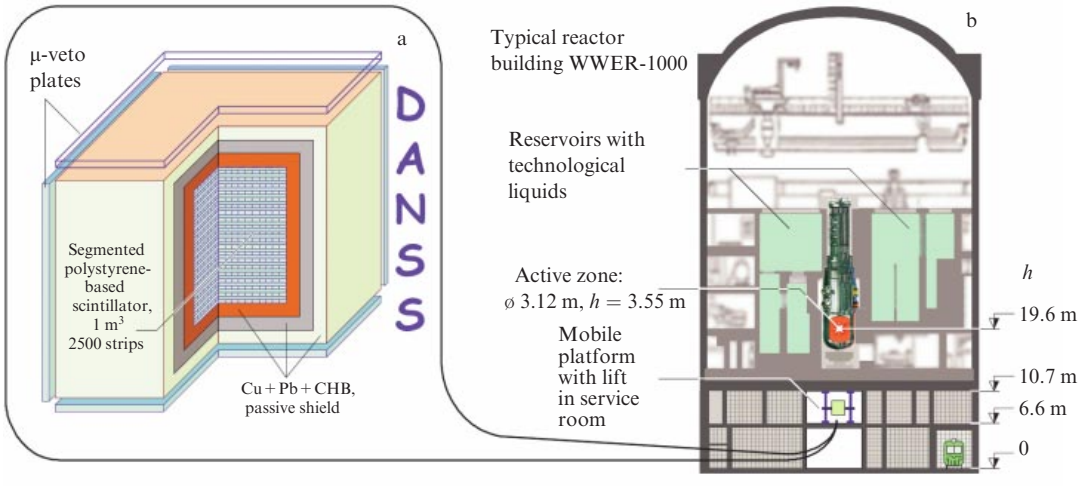

Figure 19. (a) Schematics of the DANSS neutrino detector and (b) its location under the industrial reactor WWER-1000. (CHB — armored polyethylene, WWER — water–water energy reactor.)

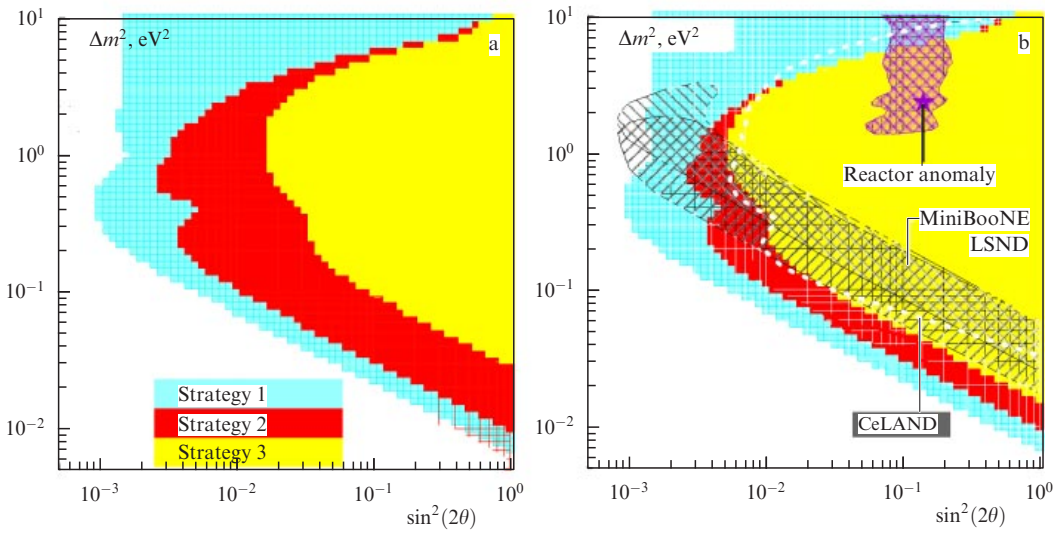

Figure 20. (Color online.) Estimate of the DANSS experiment sensitivity to oscillation parameters for one year of data collection (90% CL): (a) for an immobile detector at the central position, (b) for a detector taking data consecutively in three positions: above, at the center of, and below the reactor. The hatched areas correspond to the LSND and MiniBooNE results [99] and to the reactor anomaly [197]. The area bounded by the dashed curve is the CeLAND project proposal [198].

shown in Fig. 20, which presents results of calculations for three possible strategies. As seen from Fig. 20, the first two strategies that use the calculated spectral shape are almost indistinguishable for a static and a mobile detector, while the third strategy triples the detector sensitivity.

The νGEN experiment. The reaction of coherent scattering on nuclei $\nu + A \to \nu + A$ has not been experimentally observed so far. Coherent neutrino scattering on a nucleus occurs via the Z^0-boson exchange between the neutrino and all nucleons.

The differential cross section of this process is [200]

$$\frac{d\sigma}{d\Omega} = \frac{G_F^2}{4\pi^2} E_\nu^2 (1 + \cos\theta) \frac{\left[N - (1 - 4\sin^2\theta_W)Z\right]^2}{4} F^2(Q^2), \quad (23)$$

where θ is the angle between the neutrino incident direction and the scattered nucleus motion, N and Z are the number of neutrons and protons in the nucleus, θ_W is the Weinberg angle, and $F(Q^2)$ is the nucleus form factor. In [200], the nucleus form factor was ignored.

Because the value of $\sin^2\theta_W$ is close to 1/4, cross section (23) weakly depends on the charge of the nucleus, and after integrating (23) over the angle θ, we obtain the approximate formula

$$\sigma \simeq \frac{G_F^2}{4\pi} N^2 E_\nu^2 \simeq 0.42 \times 10^{-44} N^2 \frac{E_\nu^2}{1\ \text{MeV}^2}\ \text{cm}^2,$$

which suggests that the more neutrons are contained in a nucleus, the larger the coherent scattering cross section is.

The mean energy of the recoil nucleus with an atomic mass A is

$$\bar{E}_A = \frac{2}{3A}\left(\frac{E_\nu}{1\ \text{MeV}}\right)^2 [\text{keV}].$$

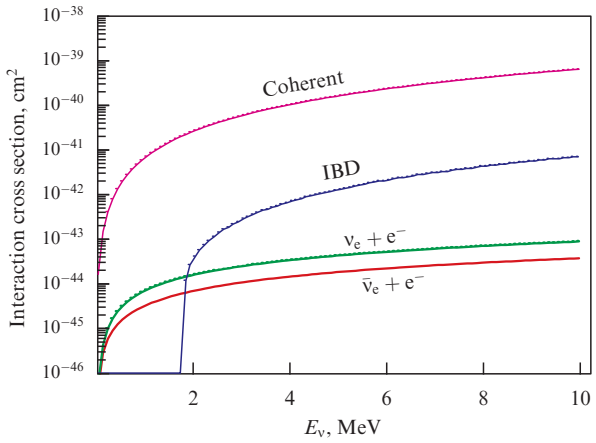

Figure 21. Neutrino interaction cross sections σ_ν in different processes.

For neutrino energies of about 6 MeV and a germanium nucleus, $\bar{E}_A \simeq 360$ eV. To register such a low energy, detectors with an extremely low energy threshold are needed.

Comparisons of cross sections of the coherent neutrino interaction with germanium nuclei with that of the inverse beta decay on a proton (for antineutrinos) and that of elastic scattering are presented in Fig. 21. It is seen that the cross section of coherent neutrino scattering on a Ge nucleus is three orders of magnitude higher than that of the inverse beta decay.

Coherent neutrino scattering is especially important from the practical standpoint, because very heavy mass detectors are typically used for neutrino detection. The comparatively large coherent scattering cross section lowers the requirements for the mass of the detector for neutrino detection in this process.

It is planned that the νGEN experiment will use low-threshold, low-background HPG (High Purity Germanium) detectors designed by JINR for the device to observe coherent neutrino scattering on Ge nuclei [201].

One of the reactors at the Kalinin NPP will be used as the neutrino source. To separate the coherent scattering contribution, the data accumulated with the reactor switched on and switched off (the differential method) will be analyzed. With a device consisting of 450 g HPGe detectors placed about 10 m from the reactor center, several dozen events a day are expected from coherent scattering with an energy threshold of 300 eV.

The sensitivity of the installation can be increased by increasing the mass of the detectors to 5 kg. The unique properties of the proposed HPGe detectors, as well as the high antineutrino fluxes available at the Kalinin NPP, make it highly probable that neutrino–nucleon coherent scattering will be observed in the νGEN experiment for the first time.

4. Conclusion

Presently, hopes to find the new physics in particle physics beyond the SM are associated with neutrinos. Of key importance here are studies of the fundamental properties of neutrinos, including possible nonstandard interactions, neutrino masses, mixing features, searches for sterile neutrinos, an answer to the question of whether the neutrino is a Majorana or a Dirac particle, and an understanding of the electromagnetic or other 'exotic' properties of the neutrinos. Some assumptions on the sources of astrophysical neutrinos discovered by the IceCube experiment are also related to the new physics. Neutrino physics today is indeed a key interdisciplinary field connecting the physics of elementary particles, cosmology, and astrophysics.

The nonzero neutrino mass is important for modern theories of elementary particles and for explaining the structure of the Universe (for example, the neutrino mass is important for the formation of the large-scale structure of the Universe). Neutrinos can play the role of hot dark matter.

Neutrino properties are responsible for the explanation of the solar and atmospheric neutrino deficit: they play a role in supernova explosion mechanisms and power production in stars (in particular, in the Sun) and inside Earth and can be important in searches for the sources of ultra-high-energy cosmic rays. Only with neutrinos can we probe the most distant parts of the Universe. Thus far, no relic neutrinos, which are likely to be the oldest elementary particles in the Universe, have been found. Alongside photons, neutrinos are the most abundant particles in the Universe. Massive neutrino CP-violating decays are thought to be able to provide the long-sought insights into the baryonic asymmetry of the Universe, i.e., the observed excess of baryons over antibaryons. Only all-penetrating neutrinos and antineutrinos are able to probe unprecedentedly large distance scales, from very small to huge distances comparable to the size of the visible Universe. Neutrinos enable us to learn what happens in the solar and terrestrial interiors, inside an exploding supernova, in an NPP reactor or in distant cosmic objects.

Applied neutrino studies have unique prospects. Recently, geoneutrinos from the terrestrial interior were detected. Their exploration is very important for geophysics to explain physical processes inside our planet and, hence, to understand the origin of various natural cataclysms and climate changes.

Applied research of reactor antineutrinos has reached a new level. It is aimed at continuously measuring the reactor power and the degree of burn-out, and performing tomography of the burning-out of fuel in real time; at constructing compact antineutrino detectors for remote control of processing and unauthorized tapping of plutonium from running a reactor, and so on.

This is the most lucid example of the practical application of fundamental science. Neutrino physics stimulates the development of new and unique technologies and detectors, which turn out to be required in other fields and ordinary life.

It is well known that after the Higgs boson was discovered at the LHC and the mixing angle θ_{13} was measured in the Daya Bay and RENO experiments (2012), the most impressive result was obtained in the Antarctic ice by the international IceCube collaboration, which detected the first ultra-high-energy extraterrestrial neutrinos of galactic and possibly even extragalactic origin.

Neutrino physics and astrophysics, together with accelerator physics of ultra-high-energy elementary particles, are the main avenues of modern elementary particle physics. These fields are especially rich in potentially the most fundamental and unexpected discoveries, which can undoubtedly change our knowledge about the world. It can be asserted that neutrino physics entered the phase of precision measurements, of systematically solving the fundamental problems on the nature of the neutrino, and this is why it is 'doomed to success'.

Acknowledgments
We are grateful to all our colleagues from JINR, Russia, and all over the world for the useful discussions. Special thanks go to V A Naumov, who read the manuscript and made valuable remarks. We are thankful to J Cao for Fig. 13.

References

1. Kudenko Yu G *Phys. Usp.* **57** 462 (2014); *Usp. Fiz. Nauk* **184** 502 (2014)
2. Spiering Ch *Phys. Usp.* **57** 470 (2014); *Usp. Fiz. Nauk* **184** 510 (2014)
3. Barabash A S *Phys. Usp.* **57** 482 (2014); *Usp. Fiz. Nauk* **184** 524 (2014)
4. Bilenky S M *Phys. Usp.* **57** 489 (2014); *Usp. Fiz. Nauk* **184** 531 (2014)
5. Olshevskiy A G *Phys. Usp.* **57** 497 (2014); *Usp. Fiz. Nauk* **184** 539 (2014)
6. Gorbunov D S *Phys. Usp.* **57** 503 (2014); *Usp. Fiz. Nauk* **184** 545 (2014)
7. Derbin A V *Phys. Usp.* **57** 512 (2014); *Usp. Fiz. Nauk* **184** 555 (2014)
8. Kudenko Yu G *Phys. Usp.* **54** 549 (2011); *Usp. Fiz. Nauk* **181** 569 (2011)
9. Troitsky S V *Phys. Usp.* **55** 72 (2012); *Usp. Fiz. Nauk* **182** 77 (2012)
10. Pais A *Inward Bound: of Matter and Forces in the Physical World* (New York: Oxford Univ. Press, 1986)
11. Cowan C L (Jr.), Reines F *Phys. Rev.* **107** 528 (1957)
12. Danby G et al. *Phys. Rev. Lett.* **9** 36 (1962)
13. Kodama K et al. (DONUT Collab.) *Phys. Lett. B* **504** 218 (2001); hep-ex/0012035
14. Kodama K et al. (DONuT Collab.) *Phys. Rev. D* **78** 052002 (2008); arXiv:0711.0728
15. Wu C S et al. *Phys. Rev.* **105** 1413 (1957)
16. Cleveland B T et al. *Astrophys. J.* **496** 505 (1998)
17. Rubakov V A *Phys. Usp.* **55** 949 (2012); *Usp. Fiz. Nauk* **182** 1017 (2012)
18. Giunti C, Kim C W, Lee U W *Phys. Lett. B* **274** 87 (1992)
19. De Leo S, Nishi C C, Rotelli P P *Int. J. Mod. Phys. A* **19** 677 (2004)
20. Bernardini A E, De Leo S *Phys. Rev. D* **70** 053010 (2004)
21. Shirokov M I, Naumov V A *Old New Concepts Phys.* **4** 121 (2007)
22. Fuji C et al., hep-ph/0612300
23. Kayser B, Kopp J, arXiv:1005.4081
24. Beuthe M *Phys. Rep.* **375** 105 (2003)
25. Giunti C, Kim C W *Fundamentals of Neutrino Physics and Astrophysics* (Oxford: Oxford Univ. Press, 2007)
26. Grimus W, Stockinger P *Phys. Rev. D* **54** 3414 (1996)
27. Cardall C Y *Phys. Rev. D* **61** 073006 (2000)
28. Akhmedov E K, Kopp J *JHEP* (04) 008 (2010)
29. Naumov D V, Naumov V A *Russ. Phys. J.* **53** 549 (2010); *Izv. Vyssh. Uchebn. Zaved. Fiz.* (6) 5 (2010)
30. Naumov D V, Naumov V A *J. Phys. G* **37** 105014 (2010)
31. Akhmedov E K *JHEP* (09) 116 (2007)
32. Ashie Y et al. (The Super-Kamiokande Collab.) *Phys. Rev. Lett.* **93** 101801 (2004)
33. Abe S et al. (The KamLAND Collab.) *Phys. Rev. Lett.* **100** 221803 (2008)
34. An F P et al. (Daya Bay Collab.) *Phys. Rev. Lett.* **112** 061801 (2014)
35. Wolfenstein L *Phys. Rev. D* **17** 2369 (1978)
36. Mikheev S P, Smirnov A Yu *Sov. J. Nucl. Phys.* **42** 913 (1985); *Yad. Fiz.* **42** 1441 (1985)
37. Maltoni M, Smirnov A Yu *Eur. Phys. J.* **52** 87 (2016); arXiv:1507.05287
38. Capozzi F et al. *Phys. Rev. D* **89** 093018 (2014)
39. Olive K A et al. (Particle Data Group) *Chinese Phys. C* **38** 090001 (2014)
40. Schael S et al. (The ALEPH Collab., The DELPHI Collab., The L3 Collab., The OPAL Collab., The SLD Collab.) *Phys. Rep.* **427** 257 (2006); hep-ex/0509008
41. Ade P A R et al. (Planck Collab.), arXiv:1502.01589
42. Aseev V N et al. (Troitsk Collab.) *Phys. Rev. D* **84** 112003 (2011)
43. Assamagan K et al. *Phys. Rev. D* **53** 6065 (1996)
44. Barate R et al. (ALEPH Collab.) *Eur. Phys. J. C* **2** 395 (1998)
45. Thomas S A, Abdalla F B, Lahav O *Phys. Rev. Lett.* **105** 031301 (2010)
46. Battye R A, Moss A *Phys. Rev. Lett.* **112** 051303 (2014)
47. Gando A et al. (KamLAND-Zen Collab.) *Phys. Rev. Lett.* **110** 062502 (2013)
48. Auger M et al. (EXO Collab.) *Phys. Rev. Lett.* **109** 032505 (2012)
49. Minkowski P *Phys. Lett. B* **67** 421 (1977)
50. Mohapatra R N, Senjanović G *Phys. Rev. Lett.* **44** 912 (1980)
51. Giunti C, Studenikin A *Rev. Mod. Phys.* **87** 531 (2015)
52. Raffelt G G *Phys. Rep.* **320** 319 (1990)
53. Arceo-Díaz S et al. *Astropart. Phys.* **70** 1 (2015)
54. Balantekin A B, Vassh N *Phys. Rev. D* **89** 073013 (2014)
55. Derbin A V *Phys. Atom. Nucl.* **57** 222 (1994); *Yad. Fiz.* **57** 236 (1994)
56. Li H B et al. (TEXONO Collab.) *Phys. Rev. Lett.* **90** 131802 (2003)
57. Daraktchieva Z et al. (MUNU Collab.) *Phys. Lett. B* **615** 153 (2005)
58. Beda A G et al. *Phys. Part. Nucl. Lett.* **10** 139 (2013); *Pis'ma Fiz. Elem. Chastits At. Yadra* **10** 217 (2013)
59. Arpesella C et al. (Borexino Collab.) *Phys. Rev. Lett.* **101** 091302 (2008)
60. Derbin A V (Borexino Collab.) *Phys. Atom. Nucl.* **73** 1935 (2010); *Yad. Fiz.* **73** 1987 (2010)
61. Auerbach L B et al. (LSND Collab.) *Phys. Rev. D* **63** 112001 (2001)
62. Schwienhorst R et al. (DONUT Collab.) *Phys. Lett. B* **513** 23 (2001)
63. Perrin F *Comptes Rendus* **197** 1625 (1933)
64. Fermi E *Z. Phys.* **88** 161 (1934)
65. Alvarez L W, Cornog R *Phys. Rev.* **56** 613 (1939)
66. Hanna G C, Pontecorvo B *Phys. Rev.* **75** 983 (1949)
67. Curran S C, Angus J, Cockroft A L *Phys. Rev.* **76** 853 (1949)
68. Kraus C et al. *Eur. Phys. J. C* **40** 447 (2005)
69. Drexlin G et al. *Adv. High Energy Phys.* **2013** 293986 (2013)
70. Angrik J et al. (KATRIN Collab.), KATRIN Design Report 2004 FZKA-7090 (Karlsruhe: Forschungszentrum Karlsruhe GmbH, 2005)
71. Li Y-F et al. *Phys. Rev. D* **88** 013008 (2013); arXiv:1303.6733
72. An F et al. (JUNO Collab.) *J. Phys. G* **43** 030401 (2016); arXiv:1507.05613
73. Kim S-B, arXiv:1412.2199
74. Ayres D S et al. (NOvA Collab.), hep-ex/0503053
75. Akiri T et al. (LBNE Collab.), arXiv:1110.6249
76. Aartsen M G et al. (IceCube-PINGU Collab.), arXiv:1401.2046
77. Ribordy M, Smirnov A Yu *Phys. Rev. D* **87** 113007 (2013)
78. Huber P, Maltoni M, Schwetz T *Phys. Rev. D* **71** 053006 (2005)
79. INO. India-based Neutrino Observatory, http://www.ino.tifr.res.in/ino//index.php
80. Blennow M et al. *JHEP* (03) 028 (2014)
81. Adams C et al. (LBNE Collab.), arXiv:1307.7335
82. Goeppert-Mayer M *Phys. Rev.* **48** 512 (1935)
83. Majorana E Il *Nuovo Cimento* **14** (4) 171 (1937)
84. Furry W H *Phys. Rev.* **56** 1184 (1939)
85. Klapdor-Kleingrothaus H V et al. *Phys. Lett. B* **586** 198 (2004)
86. Klapdor-Kleingrothaus H V, Krivosheina I V *Mod. Phys. Lett. A* **21** 1547 (2006)
87. Klapdor-Kleingrothaus H V, Dietz A, Krivosheina I V, in *Dark Matter in Astro- and Particle Physics, Proc. of the Intern. Conf., DARK 2002, Cape Town, South Africa, 4–9 February 2002* (Eds H V Klapdor-Kleingrothaus, R D Viollier) (Berlin: Springer, 2002) p. 404
88. Feruglio F, Strumia A, Vissani F *Nucl. Phys. B* **637** 345 (2002)
89. Agostini M et al. (GERDA Collab.) *Phys. Rev. Lett.* **111** 122503 (2013)
90. Bilenky S M, Giunti C *Mod. Phys. Lett. A* **27** 1230015 (2012)
91. Schechter J, Valle J W F *Phys. Rev. D* **25** 2951 (1982)
92. Aguilar A et al. (LSND Collab.) *Phys. Rev. D* **64** 112007 (2001); hep-ex/0104049
93. Aguilar-Arevalo A A et al. (MiniBooNE Collab.) *Phys. Rev. Lett.* **110** 161801 (2013); arXiv:1207.4809; arXiv:1303.2588
94. Abdurashitov J N et al. (SAGE Collab.) *Phys. Rev. Lett.* **77** 4708 (1996)
95. Abdurashitov J N et al. (SAGE Collab.) *Phys. Rev. C* **73** 045805 (2006)
96. Anselmann P et al. (GALLEX Collab.) *Phys. Lett. B* **342** 440 (1995)

97. Kaether F et al. *Phys. Lett. B* **685** 47 (2010)
98. Mention G et al. *Phys. Rev. D* **83** 073006 (2011)
99. Abazajian K N et al., arXiv:1204.5379
100. Bellini G et al. *JHEP* (08) 038 (2013)
101. Veretenkin E P et al. (Best Collab.), http://www.inr.ru/rus/bno/best.pdf
102. National Research Center 'Kurchatov Institute' Petersburg Nuclear Physics Institute. Reactor PIK, http://www.pnpi.spb.ru/eng/facil/pik.htm
103. Construction and physical features of the CM-3 reactor, http://www-dev.niiar.ru/ork/sm/features.htm (in Russian)
104. Derbin A V, Kayunov A S, Muratova V N, arXiv:1204.2449
105. Danilov M (DANSS Collab.) *PoS EPS HEP2013* 493 (2013); arXiv:1311.2777
106. Alekseev I et al. *Phys. Part. Nucl. Lett.* **11** 473 (2014); *Pis'ma Fiz. Elem. Chastits At. Yadra* **11** 735 (2014)
107. Serebrov A P et al., arXiv:1310.5521
108. Abdurashitov J N et al. (SAGE Collab.) *Phys. Rev. C* **80** 015807 (2009); arXiv:0901.2200
109. Bellini G et al. (BOREXINO Collab.) *Nature* **512** 383 (2014)
110. Bellini G et al. (Borexino Collab.) *Phys. Rev. Lett.* **108** 051302 (2012); arXiv:1110.3230
111. Bellini G et al. *Phys. Rev. Lett.* **107** 141302 (2011)
112. Aharmim B et al. (SNO Collab.) *Phys. Rev. C* **81** 055504 (2010)
113. Aharmim B et al. (SNO Collab.) *Astrophys. J.* **653** 1545 (2006)
114. Grevesse N, Sauval A J *Space Sci. Rev.* **85** 161 (1998)
115. Asplund M et al. *Annu. Rev. Astron. Astrophys.* **47** 481 (2009); arXiv:0909.0948
116. Serenelli A M, Haxton W C, Pena-Garay C *Astrophys. J.* **743** 24 (2011)
117. Lozza V (for the SNO+ Collab.) *J. Phys. Conf. Ser.* **375** 042050 (2012)
118. Hirata K S et al. *Phys. Rev. D* **38** 448 (1988)
119. Bionta R M et al. *Phys. Rev. Lett.* **58** 1497 (1987)
120. Alekseev E N et al. *Sov. Astron. Lett.* **14** 41 (1988); *Pis'ma Astron. Zh.* **14** 99 (1988)
121. Aglietta M et al. *Europhys. Lett.* **3** 1315 (1987)
122. Dadykin V L et al. *JETP Lett.* **45** 593 (1987); *Pis'ma Zh. Eksp. Teor. Fiz.* **45** 464 (1987)
123. Dadykin V L, Zatsepin G T, Ryazhskaya O G *Sov. Phys. Usp.* **32** 459 (1989); *Usp. Fiz. Nauk* **158** 139 (1989)
124. Imshennik V S, Ryazhskaya O G *Astron. Lett.* **30** 14 (2004); *Pis'ma Astron. Zh.* **30** 17 (2004)
125. Antonioli P et al. *New J. Phys.* **6** 114 (2004)
126. Aartsen M G et al. (IceCube Collab.) *Science* **342** 1242856 (2013); arXiv:1311.5238
127. Aartsen M G et al. (IceCube Collab.) *Phys. Rev. D* **91** 022001 (2015); arXiv:1410.1749
128. Bagley P et al. (KM3NeT Consortium), http://www.km3net.org/TDR/KM3NeTprint.pdf (2011)
129. Aguilar J A et al. *Nucl. Instrum. Meth. Phys. Res. A* **656** 11 (2011)
130. Davies J H, Davies D R *Solid Earth* **1** (1) 5 (2010)
131. Gando A et al. (KamLAND Collab.) *Phys. Rev. D* **88** 033001 (2013)
132. Agostini M et al. (Borexino Collab.) *Phys. Rev. D* **92** 031101(R) (2015); arXiv:1506.04610
133. Bellini G et al. *Phys. Lett. B* **722** 295 (2013)
134. Strati V et al., arXiv:1412.3324
135. Zeldovich Ya B, Gershtein S S, Dunaitsev A F, Prokoshkin Yu D, Rykalin V I, Petrukhin V I, State Register of Discoveries of USSR, Patent No. 135. Priority of 8.06.1955 (1973)
136. Pontecorvo B *Sov. Phys. JETP* **10** 1236 (1960); *Zh. Eksp. Teor. Fiz.* **37** 1751 (1959)
137. Zaimidoroga O A et al. *Sov. Phys. JETP* **18** 1235 (1964); *Zh. Eksp. Teor. Fiz.* **45** 1803 (1963)
138. Bystritskii V M *Sov. Phys. JETP* **39** 19 (1974); *Zh. Eksp. Teor. Fiz.* **66** 43 (1974)
139. Vylov Ts D et al., Preprint R6-84-148 (Dumna: JINR, 1984)
140. Pontecorvo B *Sov. Phys. JETP* **6** 429 (1958); *Zh. Eksp. Teor. Fiz.* **33** 549 (1957)
141. Pontecorvo B *Sov. Phys. JETP* **7** 172 (1958); *Zh. Eksp. Teor. Fiz.* **34** 247 (1958)
142. Baranov V A et al. *Sov. J. Nucl. Phys.* **53** 802 (1991); *Yad. Fiz.* **53** 1302 (1991)
143. Gordeev V A et al. *JETP Lett.* **57** 270 (1993); *Pis'ma Zh. Eksp. Teor. Fiz.* **57** 262 (1993)
144. Gordeev V A et al. *JETP Lett.* **59** 589 (1994); *Pis'ma Zh. Eksp. Teor. Fiz.* **59** 565 (1994)
145. Pontecorvo B *Sov. Phys. Usp.* **26** 1087 (1983); *Usp. Fiz. Nauk* **141** 675 (1983)
146. Bilen'kii S M, Pontecorvo B *Sov. Phys. Usp.* **20** 776 (1977); *Usp. Fiz. Nauk* **123** 181 (1977)
147. Dzhelepov V P, Pontecorvo B M *Usp. Fiz. Nauk* **64** 15 (1958)
148. Pontecorvo B M *Sov. Phys. Usp.* **6** 1 (1963); *Usp. Fiz. Nauk* **79** 3 (1963)
149. Pontecorvo B M *Sov. Phys. Usp.* **11** 528 (1969); *Usp. Fiz. Nauk* **95** 517 (1968)
150. Pontecorvo B *Sov. Phys. Usp.* **14** 235 (1971); *Usp. Fiz. Nauk* **104** 3 (1971)
151. Pontecorvo B *Sov. Phys. Usp.* **19** 666 (1976); *Usp. Fiz. Nauk* **119** 633 (1976)
152. Pontecorvo B M *Sov. Phys. Usp.* **19** 1031 (1976); *Usp. Fiz. Nauk* **120** 705 (1976)
153. Blumlein J et al. *Phys. Lett. B* **279** 405 (1992)
154. Baranov S A et al. *Phys. Lett. B* **302** 336 (1993)
155. Anikeev V B et al. *Z. Phys. C* **70** 39 (1996)
156. Bunyatov S A, Nefedov Yu A *Phys. Atom. Nucl.* **60** 935 (1997); *Yad. Fiz.* **60** 1045 (1997)
157. Sidorov A V et al. (IHEP-JINR Neutrino Detector Collab.) *Eur. Phys. J. C* **10** 405 (1999); hep-ex/9905038
158. Alekhin S I et al. *Phys. Lett. B* **512** 25 (2001); hep-ex/0104013
159. Barabash L S et al. *Instrum. Exp. Tech.* **46** 300 (2003); *Prib. Tekh. Eksp.* **46** (3) 20 (2003)
160. Samoylov O et al. (NOMAD Collab.) *Nucl. Phys. B* **876** 339 (2013); arXiv:1308.4750
161. Kullenberg C T et al. (NOMAD Collab.) *Phys. Lett. B* **682** 177 (2009); arXiv:0910.0062
162. Lyubushkin V et al. (NOMAD Collab.) *Eur. Phys. J. C* **63** 355 (2009); arXiv:0812.4543
163. Wu Q et al. (NOMAD Collab.) *Phys. Lett. B* **660** 19 (2008); arXiv:0711.1183
164. Astier P et al. (NOMAD Collab.) *Phys. Lett. B* **570** 19 (2003); hep-ex/0306037
165. Astier P et al. (NOMAD Collab.) *Nucl. Phys. B* **621** 3 (2002); hep-ex/0111057
166. Astier P et al. (NOMAD Collab.) *Nucl. Phys. B* **611** 3 (2001); hep-ex/0106102
167. Astier P et al. (NOMAD Collab.) *Nucl. Phys. B* **588** 3 (2000)
168. Bednyakov V A, Naumov D V, in *The White Book: JINR NEUTRINO PROGRAM* (Dubna: JINR Laboratory of Nuclear Problems); http://dlnp.jinr.ru/ru/neutrino-white-book
169. Agafonova N et al. (OPERA Collab.) *Phys. Rev. Lett.* **115** 121802 (2015)
170. An F P et al. (Daya Bay Collab.) *Phys. Rev. Lett.* **115** 111802 (2015); arXiv:1505.03456
171. Cao J, in *TAUP 2015 XIV Intern. Conf. on Topics in Astroparticle and Underground Physics 7 – 11 September 2015, Torino Italy*; Zho J, private communication
172. An F P et al. (Daya Bay Collab.) *Phys. Rev. Lett.* **113** 141802 (2014); arXiv:1407.7259
173. An F P et al. (Daya Bay Collab.) *Phys. Rev. Lett.* **116** 061801 (2016); arXiv:1508.04233
174. Mueller Th A et al. *Phys. Rev. C* **83** 054615 (2011)
175. Huber P *Phys. Rev. C* **84** 024617 (2011)
176. Vogel P et al. *Phys. Rev. C* **24** 1543 (1981)
177. Schreckenbach K et al. *Phys. Lett. B* **160** 325 (1985)
178. Von Feilitzsch F, Hahn A A, Schreckenbach K *Phys. Lett. B* **118** 162 (1982)
179. Hahn A A et al. *Phys. Lett. B* **218** 365 (1989)
180. Bellini G et al. (Borexino Collab.) *Phys. Lett. B* **687** 299 (2010)
181. Bellini G et al. *Phys. Lett. B* **707** 22 (2012)
182. Bellini G et al. (Borexino Collab.) *Phys. Rev. D* **89** 112007 (2014)
183. Bellini G et al. (Borexino Collab.) *Phys. Rev. D* **82** 033006 (2010)

184. Agostini M et al. (Borexino Collab.) *Phys. Rev. D* **92** 031101 (2015)
185. Bellini G et al. (Borexino Collab.) *Phys. Rev. Lett.* **101** 091302 (2008)
186. Bellini G et al. (Borexino Collab.) *Phys. Rev. D* **85** 092003 (2012)
187. Bellini G et al. (Borexino Collab.) *Phys. Rev. C* **81** 034317 (2010)
188. Agostini M et al. (Borexino Collab.) *Phys. Rev. Lett.* **115** 231802 (2015); arXiv:1509.01223
189. Ferrari N, Fiorentini G, Ricci B *Phys. Lett. B* **387** 427 (1996)
190. Palazzo A *Mod. Phys. Lett. A* **28** 1330004 (2013)
191. BAIKAL GVD, Scientific Technical Report (2010)
192. Patterson R B (NOvA Collab.) *Nucl. Phys. Proc. Suppl.* **151** 235 (2013)
193. Patterson R, Fermlilab Seminar, http://theory.fnal.gov/jetp/ (2015)
194. Klapdor-Kleingrothaus H V et al. *Eur. Phys. J. A* **12** 147 (2001)
195. Aalseth C E et al. *Phys. Rev. D* **65** 092007 (2002)
196. Agostini M et al. (GERDA Collab.) *Eur. Phys. J. C* **75** 39 (2015)
197. Mention G et al. *J. Phys. Conf. Ser.* **408** 012025 (2013)
198. Gando A et al., arXiv:1312.0896
199. Gomez H et al. (SuperNEMO Collab.) *Nucl. Instrum. Meth. Phys. Res. A* **718** 52 (2013)
200. Drukier A, Stodolsky L *Phys. Rev. D* **30** 2295 (1984)
201. Brudanin V B et al. *Instrum. Exp. Tech.* **54** 470 (2011); *Prib. Tekh. Eksp.* (4) 27 (2011)